An Optimized Linear Lorentz-Force Actuator for Biorobotics and Needle-Free Injection

by

Nathan B. Ball

S.B. Mechanical Engineering (2005)
Massachusetts Institute of Technology

Submitted to the Department of Mechanical Engineering
in Partial Fulfillment of the Requirements for the Degree of

Master of Science in Mechanical Engineering

at the

MASSACHUSETTS INSTITUTE OF TECHNOLOGY
[June 2007]
May 2007

Signature of Author .....
Department of Mechanical Engineering
May 20, 2007

Certified by .....
Ian W. Hunter
Hastopoulos Professor of Mechanical Engineering
Thesis Supervisor

Accepted by .....
Lallit Anand
Professor of Mechanical Engineering
Chairman, Department Committee on Graduate Students

An Optimized Linear Lorentz-Force Actuator for Biorobotics and Needle-Free Injection

by

Nathan B. Ball

Submitted to the Department of Mechanical Engineering
on May 20, 2007, in Partial Fulfillment of the
Requirements for the Degree of
Master of Science in Mechanical Engineering

Abstract

Voice coils are a configuration of Linear Lorentz-force Actuator (LLA) that offer efficient transduction of electrical energy into linear motion. The simple geometry of a typical voice coil motor makes the configuration easily tunable for custom applications. Recent advances in high-energy magnets offer significant advantages in LLA performance when properly tuned. This thesis outlines the design, construction, and implementation of an optimized LLA which achieves superior performance to any commercially available linear motor of its size and mass. The actuator weighs 580 g, and produces 50 N continuously at 10 Hz through its 30 mm travel. It features integrated feedback control circuitry, making it a standalone modular system which lacks only a power source. The use of this LLA benefits many applications, including biorobotic actuation and needle-free injection. Using this LLA as an actuator for a biorobotic fish fin, higher precision motion is achieved at higher bandwidth than off the shelf alternatives. In two different needle-free injection systems, full control of injection pressure over time is enabled in a more compact package than previously possible. Finally, the LLA is implemented to drive a portable rapid-fire needle free injection device capable of delivering 2 mL/s at a 2 MPa.

Acknowledgements

Thank you to my parents for your unending support through my engineering education, from digging holes in the garden at age two to graduating with my master's at MIT. Beyond giving me the tools to learn and the unwavering support for any of my creative endeavors, your constant insistence that I always think ahead to the next step has both improved my innovative thought processes and kept me alive through the countless scenarios when a project gone awry could have had catastrophic results. I hope to serve my own children even half as well as you have me.

Thank you to Prof. Ian Hunter for asking me to join his lab, and giving me a veritable engineering rocket launcher to ride. His lab and the people in it are among MIT's finest points, and the opportunity to work here has been the defining aspect of my engineering education at MIT. This lab is the standard by which I will inevitably compare any work experience in the future.

Thank you to my incredible colleagues Tim Fofonoff and Craig Forest. Working along side you has been more of an inspiration to me than you might know, and I am grateful for your friendship. Thank you as well to my other co-workers and supervisors Andrew Taberner, James Tangorra, Cathy Hogan, Nate Wiedenman, Priam Pillai, Scott McEuen, Brian Hemond, Bryan Ruddy, and the rest of the BioInstrumentation Lab. I will miss working with you all.

And thank you Dan Walker and Bryan Schmid, my other colleagues at Atlas Devices. You two and Tim comprise the best team I have ever worked with, and I can't wait to see what we make of ourselves as a 'real' company.

Contents

Table of Figures

1.0 Introduction

Coupling high forces with both rapid and precise movements is a challenging but essential task for any state of the art actuator, and the impetus to combine these capabilities in systems of increasingly stringent volume and mass parameters is ever-present. This thesis outlines the development of an improved design of linear motor in the form of a Linear Lorentz-force Actuator (LLA, or voice coil) and its application to two areas which greatly benefit from its use: biorobotics and needle-free injection.

2.0 Linear Lorentz-Force Actuators

Lorentz-force actuators are ubiquitous. These motors in their linear form appear most commonly as voice coils, whose usual purpose is driving speaker cones in sound systems. A voice coil is shown in Figure 1A below, alongside a diagram of a speaker in Figure 1B.

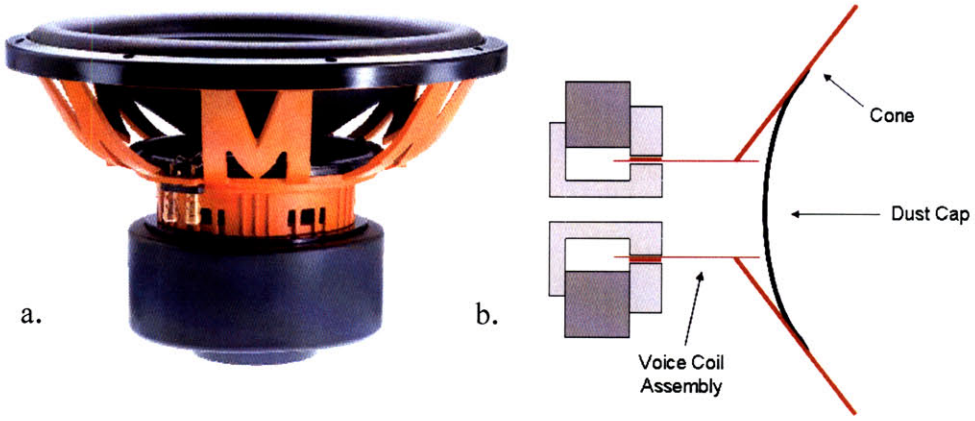

Figure 1a. Speaker with voice coil. Figure 1b. Diagram of voice coil shows air gap, magnets, core, coil, and speaker cone.

Other configurations of linear motors exist and are employed in applications including high-speed trains [2], industrial machine tools [3], and electromagnetic weapons [4].

2.1 Advantages and Limitations of the Voice Coil Configuration

The voice coil motor design is efficient and easy to manufacture. It can be scaled in different ways to vary its characteristics, making it an especially versatile configuration of electromechanical actuator. Adjusting motor parameters such as core and coil geometry, permanent magnet materials, coil gauge, and aspect ratio will vary the motor constant, maximum displacement, and bandwidth to achieve the desired characteristics.

In loudspeaker applications, voice coils are optimized for maximum bandwidth at the cost of high forces. For use in biorobotic systems or high power jet injections, much greater forces are required, but at lower bandwidth. There exist several off the shelf LLA products that would be suitable for the desired applications of this thesis, but limitations in their design prevent their optimal use. One of the higher performance actuator coils on the market is shown below in Figure 2, as produced by BEI Kimco Magnetics.

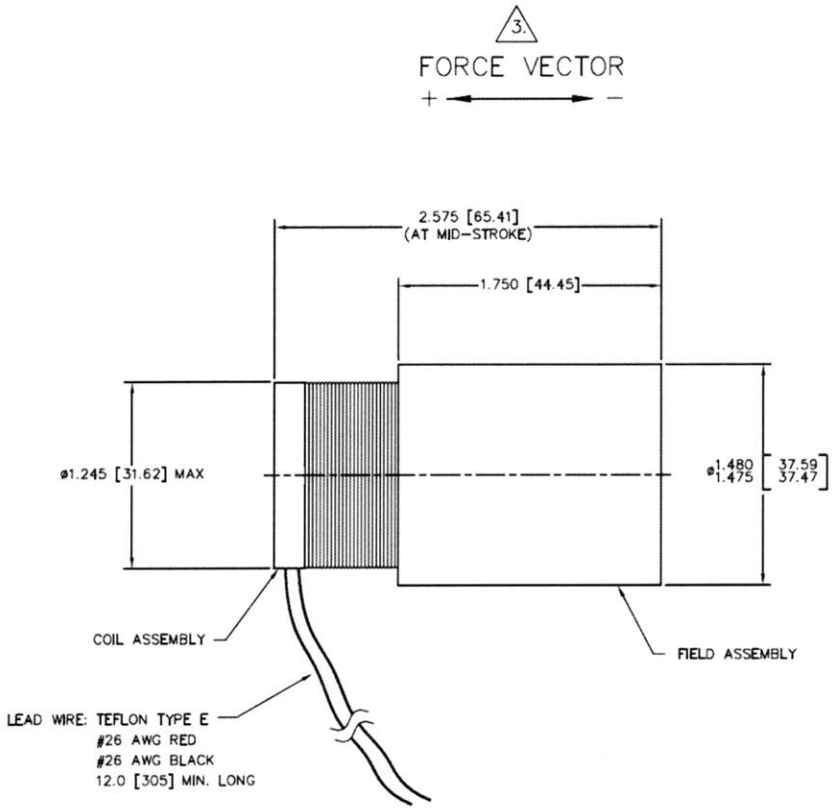

Figure 2. BEI-Kimco LA15-26-000A voice coil actuator with 25.4 mm total travel, and force constant 8.81 N/A [1].

The BEI product offers a higher force constant (8.81 N/A) due to well-designed motor geometry and Neodymium-Iron-Boron (NdFeB) magnets which produce high field strength in the gap, yielding a peak force of 50 N through its 25.4 mm of travel [1].

These parameters would be suitable as a baseline for the BEI coil's use as actuators for small biorobotic systems, including the biorobotic fish fin for which the subject of this thesis was created. The appropriate mix of force constant, bandwidth, travel, and package size make it reasonably well-suited to a range of moderate force applications with off-the-shelf driving hardware. However, to achieve the desired system performance of the biorobotic fin prototype, a higher force constant is necessary, along with a built-in linear guide system to compensate for off-axis loads.

In a developmental biorobotic system such as a robotic fin, it is desirable to utilize actuators that are modular, such that they can be used in arrays and easily reconfigured for different iterations of the fin mechanism. For these reasons, rotational hobby servos were initially selected for the prototype. Off the shelf voice coils are severely limited in modularity because of their requirement for an external bearing. For a coil to function as a plug-and-play standalone motor, a linear bearing system must be built into the core that can keep the coil assembly aligned concentrically with the core structure as the coil moves back and forth along its travel. This is typically accomplished by an application-specific guide such as air bearings built into the structure of the application itself.

Another performance limitation of off-the-shelf voice coil motors is that the spool onto which the wire is wound is often aluminum. When in motion, the back Electro-Motive Force (EMF) produced by the coil induces a magnetic field opposite that created by the forward current, and the new opposing field slows the coil's motion, reducing the bandwidth of the system. Therefore an additional performance advantage is granted to a voice coil that uses a high temperature plastic or other nonconductive material as a coil form. Eddy current damping is prevented and the moving coil's mass is reduced, increasing the system bandwidth further [11].

2.2 Theory of Lorentz-Force Actuators

The force produced by any Lorentz-force actuator is governed by

$$F = B \times i \ , \qquad 1$$

where F is force (N), B is magnetic field strength (T), and i is the current passing through the wire in the field (A). The following figure demonstrates the equation graphically with respect to a voice coil actuator. One can see from the figure that the B-field crosses the current transversely by emanating radially outward through the air gap where the coil rides.

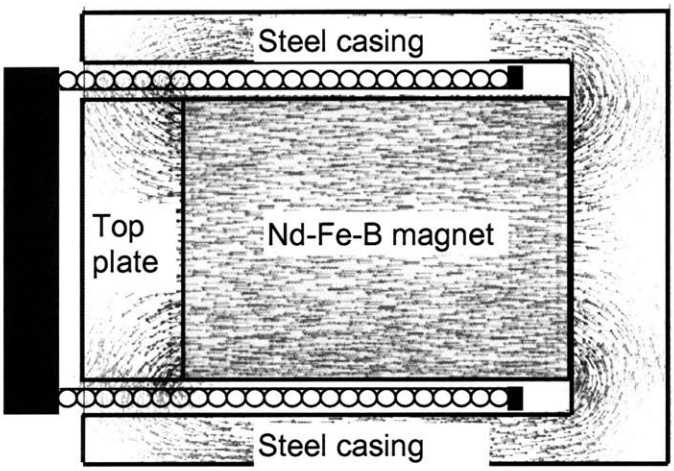

Figure 3. B-field emanating from field guide at top of core through the air gap. The field always crosses the coil orthogonal to the current, and produces force in a direction according to the cross product of the field with the current (Reproduced from Taberner *et al.* 2006).

To improve the performance of the system, it is clear that either the strength of the magnetic field or the current in the coil must be increased. This creates a challenging trade-off. If one desires the maximum force possible from the actuator at a given voltage, the only performance increase for force can come from improving the field strength. By decreasing the wire gauge which increases the number of coils in the field gap, the total length of the wire is increased and thus so is the coil resistance. At the given driving voltage then, the force is not increased because the additional voltage necessary to drive the current through that resistance decreases the current as per Ohm's law,

$$V = I \times R, \qquad 2$$

where V is the voltage, and R is the resistance of the coil. Thus for a fixed voltage, additional improvements to the performance for a given geometry are confined to increasing the field strength or optimizing the geometry for maximum performance in a narrow voltage range.

3.0 Background – Biorobotic Fish Fin

The first application-specific design of the improved Lorentz-force linear motor was for the biorobotic fish fin, which has been developed by the MIT BioInstrumentation Lab as part of a Multi-University Research Initiative (MURI) [5].

Even the most advanced Autonomous Underwater Vehicles (AUVs) of today are bulky, cumbersome, inefficient, and noisy compared to their natural counterparts. Observing the significant disparity in performance between fish and AUVs in terms of agility, maneuverability, efficiency, and stealth illuminates a clear impetus for biomimetic design [6]. By a rigorous examination of the driving factors behind fish propulsion and maneuvering, we hope to be able to recreate to whatever extent possible the ease and precision with which fish move in unsteady flows, and make it scalable and feasible for use in AUV propulsion.

To this end, we have constructed a biorobotic replica of the pectoral fin of a Bluegill Sunfish [5]. Through extensive kinematic and hydrodynamic analyses of fish swimming in unsteady currents, it has been determined that the primary low-speed propulsion and maneuvering performed by fish is in fact done so via paired pectoral fins [7]. This is in contrast to the pursuits of AUV engineers who have extensively investigated the use of body propulsion for autonomous underwater systems [8]. However, when closely examining the sources of the fish's superior positioning and maneuvering capability, we find that the dominating modes of body positioning at low velocity are from the fins [7].

Several factors account for the superior performance afforded by fin maneuvering. The fins function as conformal control surfaces that when positioned around the body, enable refined motion control with relatively little force output. With a high degree of three dimensional motion that is articulated in a flexible manner relative to the fish body, the fish is able to rapidly reorient the fin surface. This quickly generates and controls force vectors in real-time, keeping the fish stable in unsteady flows [9].

Creating a conformal surface is an exceptionally difficult task with traditional actuation and structural technology. Limitations of mass, footprint, and single-dimensional actuation per motor make the effective implementation of such a conformal surface propulsion system nearly impossible for an AUV. However, artificial muscles, and particularly conducting polymer actuators, provide a unique solution that brings such a system into much closer proximity [10]. Ultimately we aim to create a fully articulated conducting polymer-actuated fish fin that accomplishes the aforementioned goals of AUV propulsion and maneuvering. In the mean-time, while this technology has great potential but still has yet to be implemented well as an engineering actuator, we have created an in-between solution. Our biorobotic fish fin enables the exploration of our attempts at mimicking the dominant modes of conformal surface propulsion of the Bluegill Sunfish.

3.1 Biorobotic Fin Prototype

The Bluegill Sunfish was chosen as the base model for kinematic and hydrodynamic swimming analysis. It is a classic pectoral fin swimmer, which is characterized by highly agile and finely controlled positioning in an unsteady flow environment. Its pectoral fins are strong enough to rapidly propel the fish away from danger, and additionally hover, brake, rapidly reorient, and turn the fish body on a dime. An additionally notable feature of the pectoral fin swimming employed by the Bluegill is that it produces forward thrust on the recovery stroke of its pectoral fin, due to vortex shedding off the "curl" actuation mode.

The biorobotic fin prototype mimics the general construction of the Sunfish fin, which is shown schematically below in Figure 4.

a. 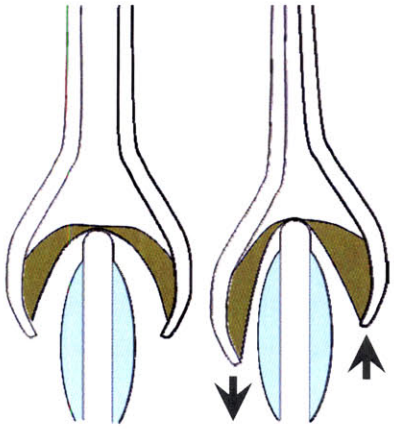 b. 

Figure 4a. The bifurcated splines, or hemitrichia, ride on a cartilage pad connected by ligaments, shown in green. This allows the hemitrichia to shift vertically with respect to one another while maintaining their connection to the cartilage below (Reproduced from S. Naomi Davidson SM2005). 4b. Bluegill Sunfish.

This anatomy is typical for a ray-finned fish such as the Bluegill.

A mechanical implementation of this mechanism is shown in Figure 5.

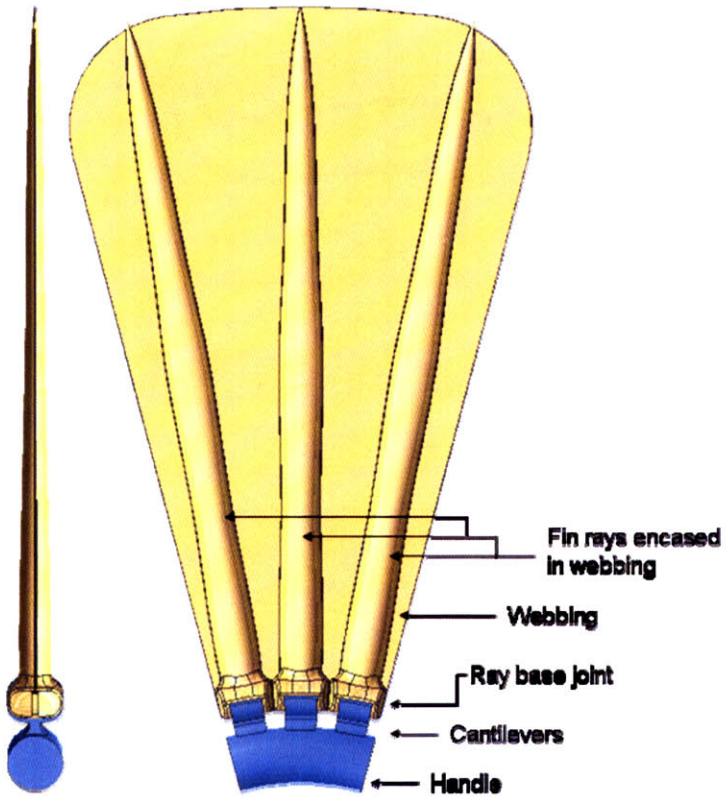

Figure 5. The hemitrichs are replicated using 3D-printed splines via stereolithography. They are hinged at the base with co-molded urethane, and spanned in-between using ligher durometer urethane to create the surface (Reproduced from S. Naomi Davidson SM2005).

For the purpose of quickly creating a functional prototype of the robotic fin, hobby servo actuators were used to pull the tendons leading to each hemitrich, as shown in Figure 6.

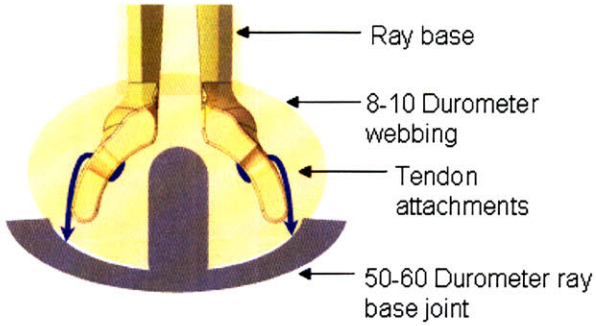

Figure 6. String tendons extend through the base joint and attach to the bases of the hemitrichs. By pulling on the tendons in an alternating fashion, the hobby servos can achieve both sweep and curl modes in each fin ray (Reproduced from S. Naomi Davidson SM2005).

3.2 Biorobotic Fin Test Modes

Though numerous orthogonal modes comprise the complete swimming motion of a Bluegill's pectoral fin 92% of the fin's total thrust can be reproduced by combining as few as three of the most energetic modes [12].

The four modes that are attempted to be reproduced by this fin are characterized as spread, cupping, curl, and sweep, and are illustrated below in Figure 7.

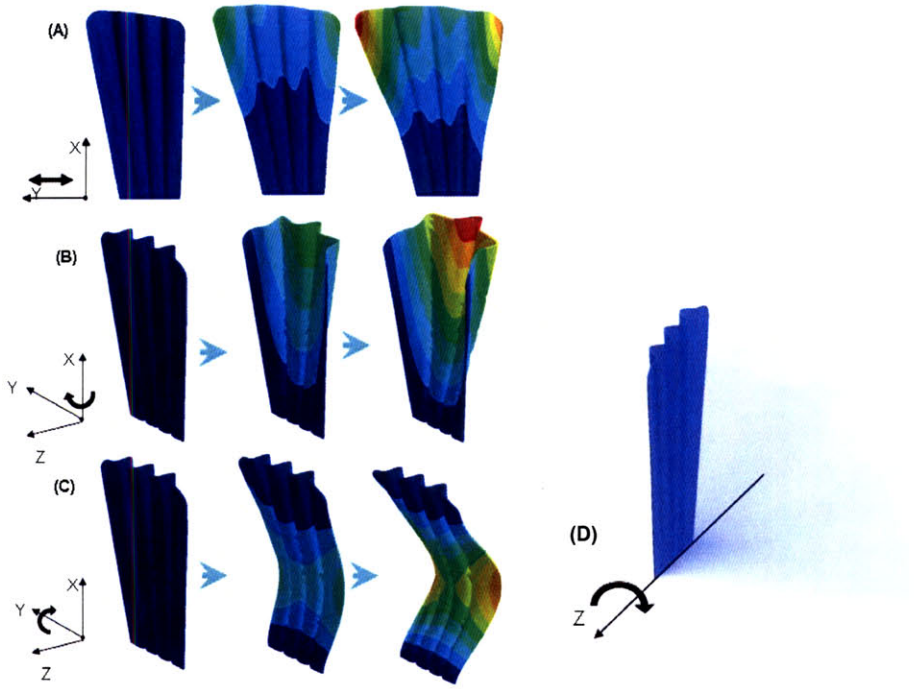

Figure 7. A visual demonstration of an idealized pectoral fin shows the modes of fin formation under spread (A), cupping (B), curling (C), and sweep (D) of the fin's surface (Reproduced from S. Naomi Davidson SM2005).

3.3 Servo-Actuated Biorobotic Fin Construction

The biorobotic fin was created with a combination of stereolithography (SLA) 3D Printing and co-molding of silicone and urethane rubbers. As mentioned before, tendons were attached to each hemitrich for actuation, as threaded through the SLA base.

Actuation was accomplished via hobby servomotors which pulled on the tendons. A close-up of a 4-ray biorobotic fin prototype is shown below.

Figure 8. 4-ray biorobotic fin prototype. Tendons at the top actuate the fin rays, which are co-molded and clamped into the urethane fin surface (Photo by James Tangorra).

Actuation modes enabled by the fin were effective in replicating their intended biological counterparts.

Figure 9 below illustrates the 3 shaping modes (not including sweep) as completed by the prototype.

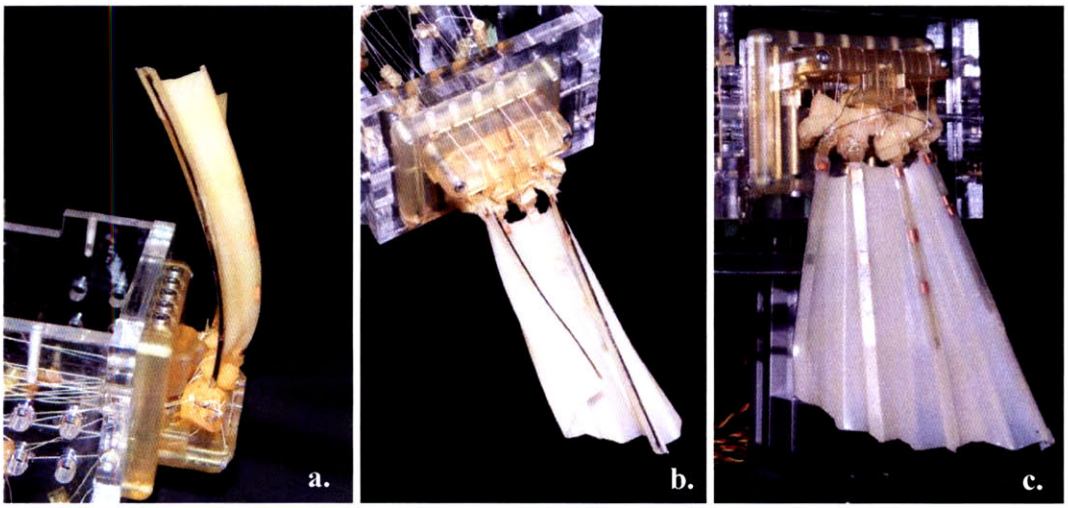

Figure 9a. Curl mode. 9b. Cupping mode. 9c. Expansion mode (Photos by James Tangorra).

3.4 Biorobotic Fin Performance

In order to evaluate the biorobotic fin's performance, it was necessary to place the entire assembly in a flow tank. For this purpose, an air bearing sled was constructed from which to suspend the fin inside the tank by a frictionless mount that enabled exact force production measurement.

3.4.1 Single-Axis Air Bearing Sled Construction

The design of the air bearing sled was driven by several important parameters. Objectives of the sled design included:

- Mount to top of flow tank while fitting within frame envelope during installation
- Submerge fin at appropriate depth
- Provide single-axis and dual-axis frictionless force measurement

- Rotate in 2 axes for adjustment of biorobotic fin orientation with respect to incoming flow
- Mount biorobotic fin into air bearing sled such that it is solidly constrained but still easily removable to facilitate maintenance

Air bearings were procured from New Way Air Bearings, with 20 mm diameter rails for the main guides. The construction of the sled body and mounting hardware consisted primarily of acrylic sections bolted together in combination with hardware from Maschinenbau-Kitz (MK). A rendered image of the CAD model is shown below.

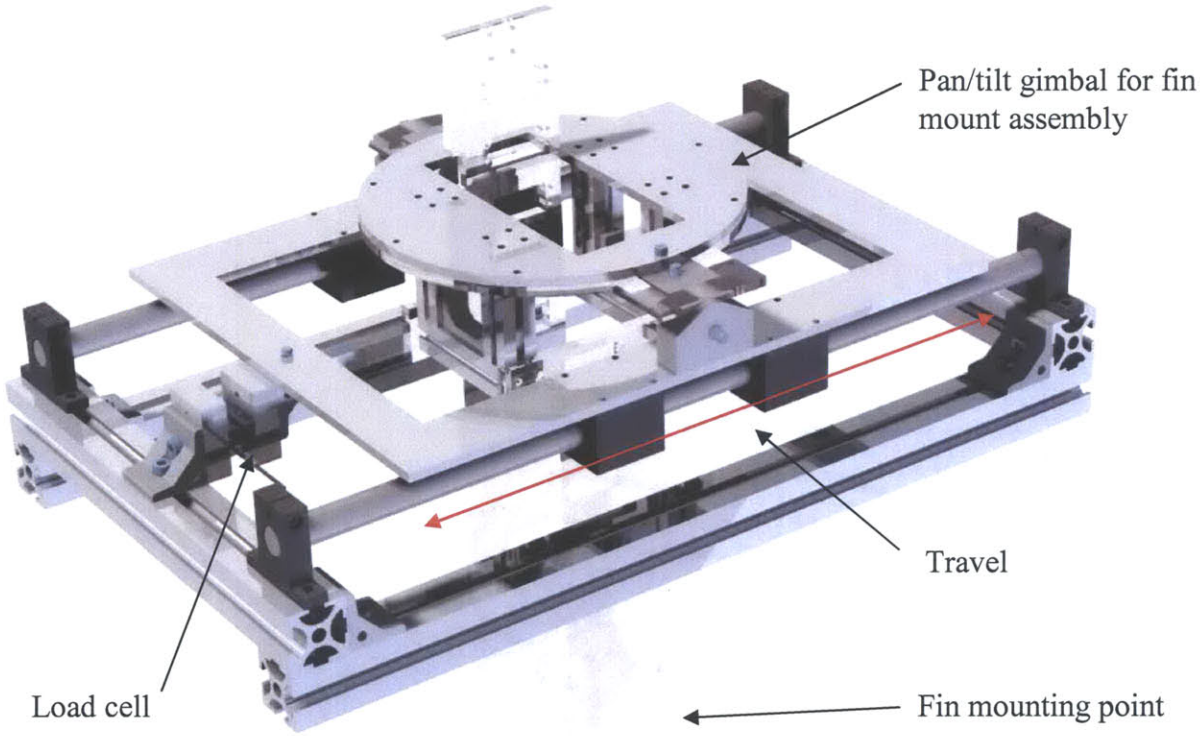

Figure 10. Frictionless air bearing sled for single-axis measurement of force in a flow tank. MK stock is used for the primary structure. Acrylic comprises the primary structure. 2-axis rotation is accomplished by the gimbal mechanism mounted on the sled portion.

In order to prevent over-constraint in the linear bearings, elastically averaged design strategies were utilized. The resulting system was effectively frictionless over its 400 mm

travel. In the flow tank the system was used statically, with a load cell locked in between the grounded frame and the frictionless sled. Thus, in the flow tank, any forces produced by the fin swimming in the flow were relayed directly to the force gauge without static or dynamic friction to account for.

3.4.2 Dual-Axis Air Bearing Sled Construction

At a later stage in the project, the need arose to use the same air bearing sled to measure thrust produced by the fin in both the surge and sway (X and Y) directions. A modification to the single-axis air bearing sled was completed which mounted the entire surge-direction sled on a second set of air bearings which were also elastically averaged to prevent over-constraint. The cad model for the resulting design is shown in Figure 11. The system was constructed and utilized to fully test 2-axis thrust production in all subsequent biorobotic fin prototypes.

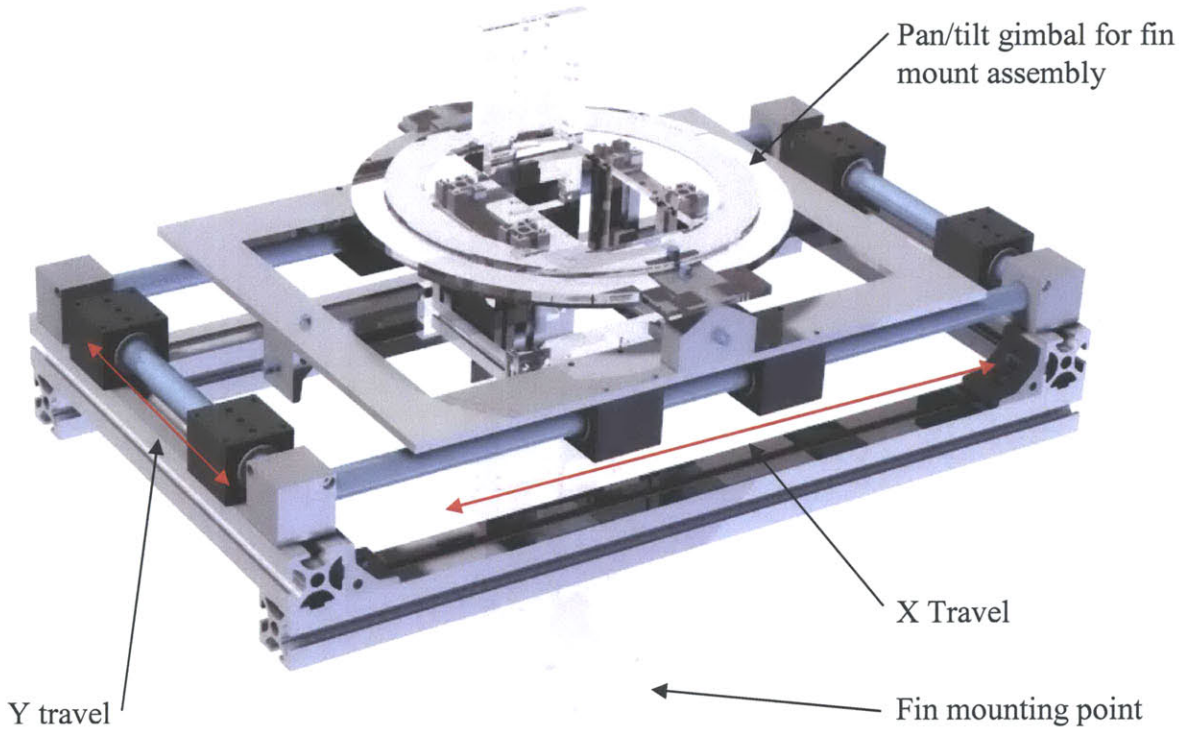

Figure 11. Two-axis frictionless air bearing sled for measurement of biorobotic fin thrust production in both the heave (X) and sway (Y) directions.

3.5 Considerations for Design of LLAs to Power Biorobotic Fin

The results of the servo-powered fin were promising. Under hobby servo actuation, the fin was able to produce measurable forward thrust as well as effectively reproduce the cupping, curling, sweep, and expansion modes as desired. But the forces produced by the system were inadequate to power an AUV, and the bandwidth of actuators prevented the system from running higher than a few hertz due to the low slew rate of the rotational hobby servos. Additionally, the servos had too low of power output, inadequate acceleration, and were noisy.

The following requirements were articulated with respect to constructing a new design of LLA to power the biorobotic fin system instead of hobby servos. The silent operation requirement was fulfilled inherently by the switch to LLAs, but the remaining requirements required extensive design iterations to fulfill.

- Silent operation
- 50 N continuous force output
- 10 Hz bandwidth
- 30 mm travel
- Greater force constant than 10 N/A
- Fully guided coil with integrated linear bearings
- Built-in control circuit for servo functionality
- Easily mountable for maximum modularity
- Easily manufactured
- Minimized mass

The following sections outline the design process that was executed in order to create a new LLA device with the desired characteristics.

3.6 Design and Fabrication of Improved LLA

Linear Lorentz-force actuators are well understood and extensively developed in many products. Improvements to their performance do not come easily, and are limited to only a few inherent advances in their construction. Otherwise, improvements in their efficacy for a given design are confined to application-specific modifications for parameters such as system integration or assembly.

3.6.1 Force Constant

Equation 1 delineates the Lorentz-force equation which governs the actuator. Clearly, in order to improve the force output per unit current of the actuator, either the field strength in the gap must improve, or the number of times the current passes through the field must increase. This solution was discussed earlier in Section 2.2.

In order to increase the force constant, improvements can only be made in optimized or exceptionally clever geometry, or use of advanced materials. Iteration 4 of the design is depicted in Figure 12 below. In order to increase the strength of the field in the air gap, Iteration 4 utilized a push-push magnet configuration with the North poles of two magnets facing each other. Thus, the field is literally squeezed into a plane of doubled intensity for a given air gap. This design has the advantage that it does not occupy extra space since the extra magnet still falls within the envelope of the coil's travel, but disadvantages include added mass and extra difficulty in attaching end effectors to the moving coil itself. A finite element approximation of the electromagnetic field in this design is shown below.

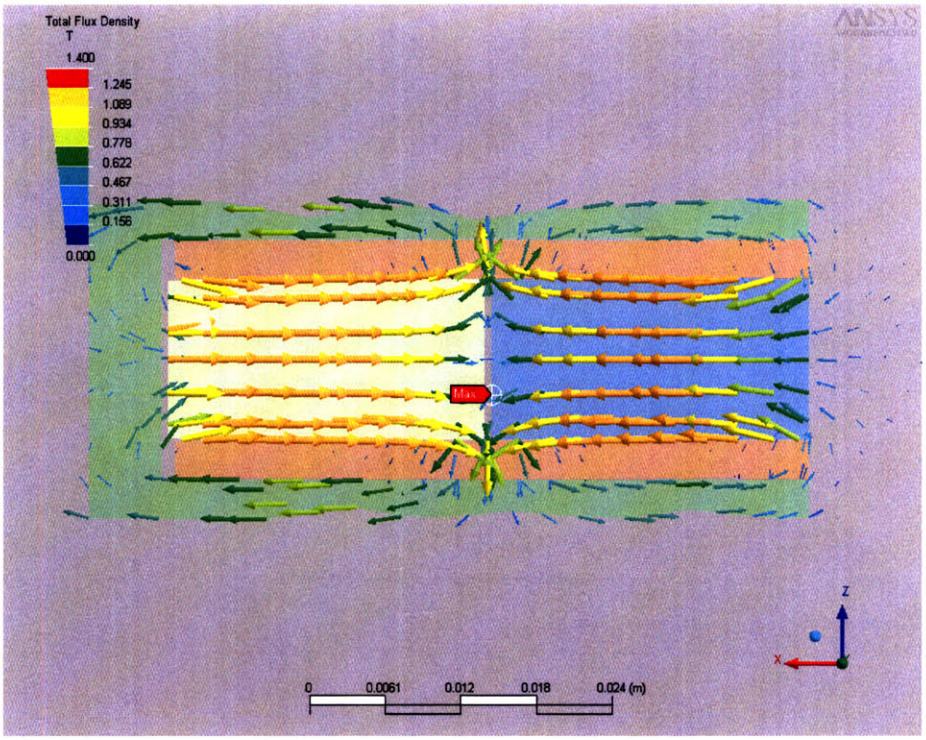

Figure 12. Field lines showing the resulting magnetic field of a double opposing-magnet design. Note the saturation in the ends of the core due to its composition of low-carbon steel. No. 1026 steel was chosen for its durability, machinability, strength, and availability. Though its magnetic permeability is not as low as the optimal materials such as pure soft iron or silicon steel, it sufficed for the purposes of this development.

Without extreme geometry conditions such as the design of Iteration 4 or other flux-shaping or flux-squeezing designs, the remaining possible improvements include shrinking the tolerance in the coil's air gap—increasing the flux—or improving the magnets used in the core to generate the permanent magnetic field.

On closer inspection, even the most state-of-the-art, off the shelf linear actuators are using lower quality magnets than are available [1]. On average, the strongest magnets utilized by Original Equipment Manufacturers (OEMs) are near $3.18*10^5$-$3.34*10^5$ J/m^3 (40-42 MGOe). Recent advances in magnet sintering technology have brought the price of even stronger magnets to within an affordable range. These magnets now have energies up to $4.05*10^5$ J/m^3 (51 MGOe), available in an N51 quality NdFeB format. The inclusion of N50 magnets in Design Iteration 13 yielded a field strength of 0.6 T in the

gap, which was over twenty percent higher than the best OEM solution. Ultimately, custom-sintered magnets were created for this application and utilized with excellent results.

3.6.2 Linear Guide

As previously mentioned, nearly all commercially available LLAs only include the actuator assembly and must be coupled with an outside guide mechanism to keep the coil aligned within the core. The desire for this system was that a linear guide bearing would be included, creating a more versatile actuator for plug-and-play applications within the biorobotic fin. A first attempt at an integrated guide bearing was created in design iteration 3, and yielded good results, though the system was less refined at that point. A picture of a prototype is shown below in Figure 13.

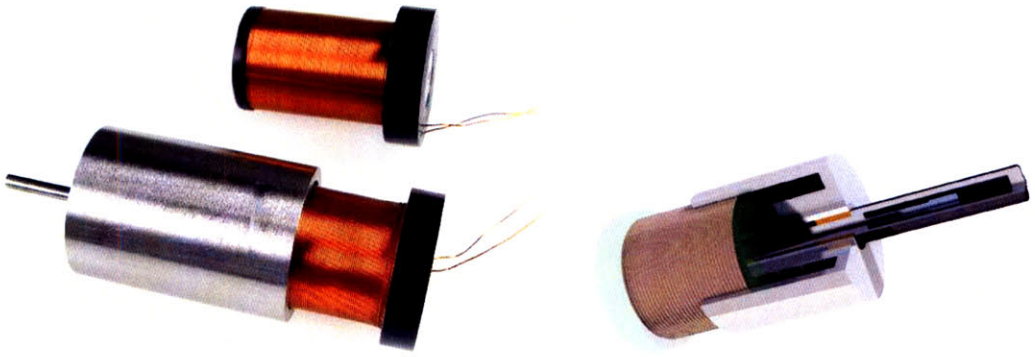

Figure 13. Design iteration 3 of the LLA, which includes a central pin as a linear guide. The CAD model on the right also shows a linear position built into the center of the core, which interfaces with the coil at the front of the former.

Problems with this design included a decreased force constant due to the magnets being cored out in the center. In order to accommodate a plastic sleeve bearing in the center of the middle core, it was necessary to increase the bore to match the press-fit of the sleeve. This decreased the amount of permanent magnet in the core, and the field strength in the air gap noticeably decreased. Additionally, the feasibility of incorporating an off-the-

shelf linear position sensor inside the middle of the core proved to be prohibitively difficult, so the iterations continued to advance.

3.6.3 Permeability

In order to decrease the mass of the system, less material in the steel core is desired. A minimum cross-sectional area is required in order to prevent saturation of the core, and thus the reduction in core thickness is limited by its permeability. Increasing the permeability of the material will enable a thinner wall, and thus reduce the weight of the assembly.

One way to increase the permeability of low-carbon steel is by annealing. By heating the steel core up to 900° C and controlling the temperature on an extremely slow cool-down, the grain structure of the steel can be realigned such that the magnetic properties are more advantageous for the desired performance. One prototype core was annealed, the visual results of which are shown in the figure below.

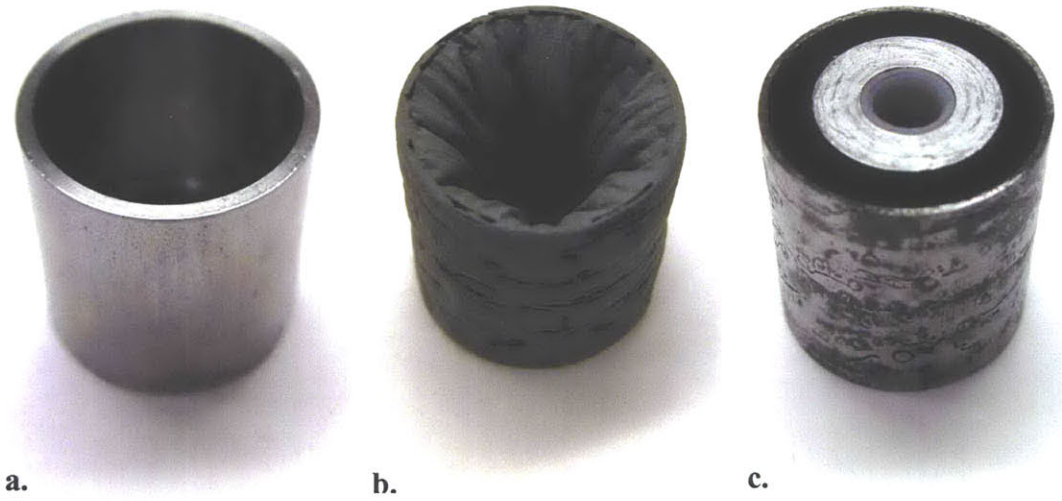

Figure 14a. A prototype core pre-annealing, 14b. immediately after annealing with carbon buildup covering the surface, and 14c. after re-assembly. In 14c., material removal in the center of the magnets facilitates a delrin sleeve that serves as a linear bearing surface—a feature that was eliminated due to decreased field strength.

The prototype annealed core was fully constructed before and after annealing, and the field strength was measured at each stage. After determining that the field strength did not appreciably increase due to the annealing, it was decided upon to no longer undergo the annealing process. Additionally, the increased ductility that resulted from the annealing processes made the press-fit interfaces less effective when assembling the magnets and other field guides, reducing the reliability of the design.

3.6.4 Design Iteration 13

Further design iterations were completed that incrementally solved the aforementioned issues. The final design that came into widest use as a turnkey actuator solution for the biorobotic fin was Design Iteration 13.

3.6.4.1 Linear Bearing

A key feature of the guide system came in reversing the planned guide system from the internal guide concept illustrated by Design Iteration 3. Greater simplicity was achieved by doing away with the spaced tolerance between the coil former and the inside of the core, and by turning that interface into the bearing surface itself. Additionally, this design improved ease of manufacture, friction and wear properties, and alignment.

In order to have the linear bearing surface be part of the coil former itself, the outer guide had to be extended forward from the core, since the inner diameter of the core then became the other half of the bearing surface. The core was extended forward, with cutouts added for access, cooling, and weight reduction, and the outer diameter of the coil former was expanded to match up with the new bearing surface.

This extended design is shown in Figure 15 below in Design Iteration 10, which was the first to incorporate this guide system.

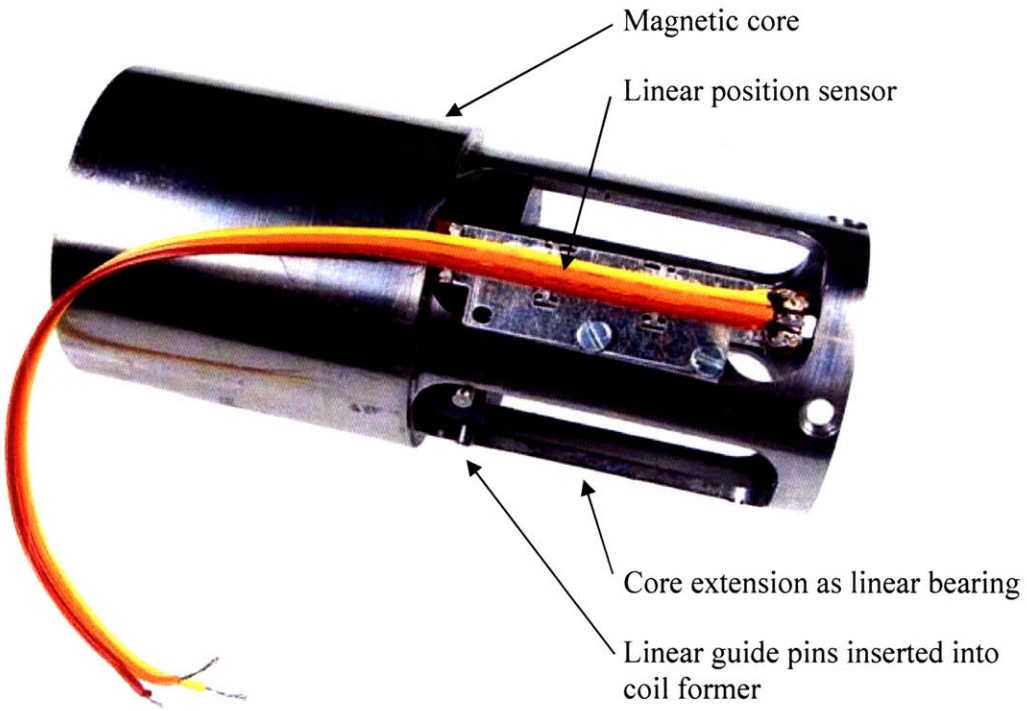

Figure 15. In Design Iteration 10 above, the extended core can be seen coming off the end of the original core extent, which is now in the middle of the device. Also, the now-integrated linear position sensor is seen on the top, as well as linear guide pins in one of the open channels.

3.6.4.2 Position Sensor Integration

As can be seen in Figure 15 above, the extent of the linear guide system provided an optimal place to mount an off the shelf linear position sensor. The 10 kΩ slide potentiometer is manufactured by Alps Sensors, and is typically manufactured for high-precision audio equipment [13].

Machining for the core was completed on a Mazak Super QuickTurn MS, which enabled both the turning operations and the milling operations that made this design possible. The potentiometer was attached to the core via its own screw holes, and aligned to center using a laser-cut acrylic tapered shim. The interface between the coil former and the position sensor was also simple, and was created by milling a small slot in the front cylinder of the coil former. The pin from the linear position sensor was inserted into the slot, which allowed a small amount of rotation to prevent over-constraint, yet snugly held the pin to maintain a high degree of positional accuracy along its sliding travel.

3.6.4.3 Linear Guide Pins

The milling operations that created pockets in the sides also created a convenient guide surface to which the coil former could be aligned. By drilling a radial hole in the coil former and inserting a dowel pin, the coil could be rotationally constrained while maintaining efficient linear motion. This was similar to the interface between the position sensor and the coil former itself.

3.6.5 Electrical System

In order to make a fully functional plug-and-play actuator that required no outside support equipment, the newly created Iteration 13 still needed to be controlled. To accomplish this, a simple position feedback servo controller was created from a 741 op-amp, the block diagram of which is illustrated below.

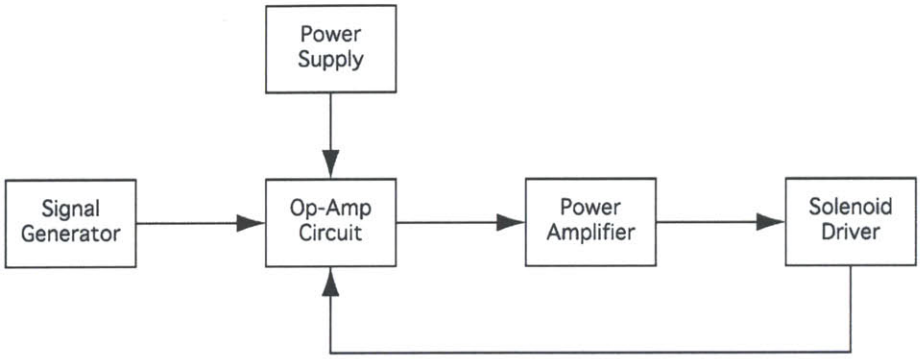

Figure 16. Proportional feedback loop for position servo control of the LLA system.

A test setup was created using an Apex PA12 amplifier which was battery powered. For simplicity, it was desirable to make the only inputs power and signal, with position and force as outputs of the system. The resulting linear servo system is shown in Figure 17 below.

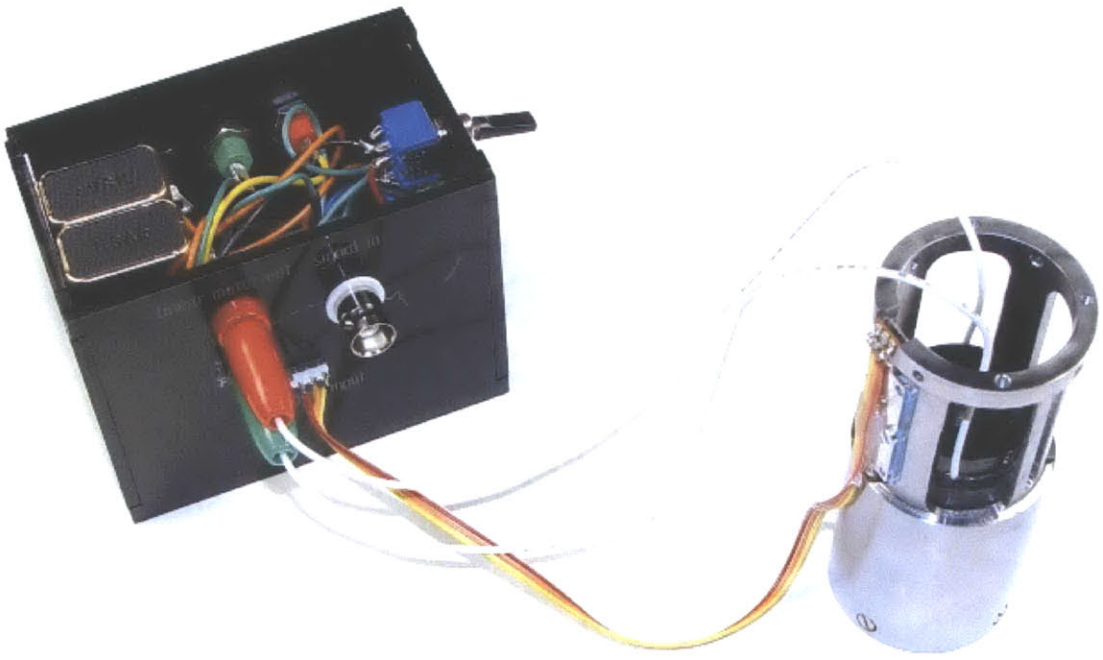

Figure 17. Design Iteration 13 is connected to an operational amplifier proportional feedback circuit. The power amp utilizes two 9 V batteries for power, and can achieve 10 N continuous force output during operation.

The circuit utilized in Design Iteration 13 is illustrated in the Figure 18 below.

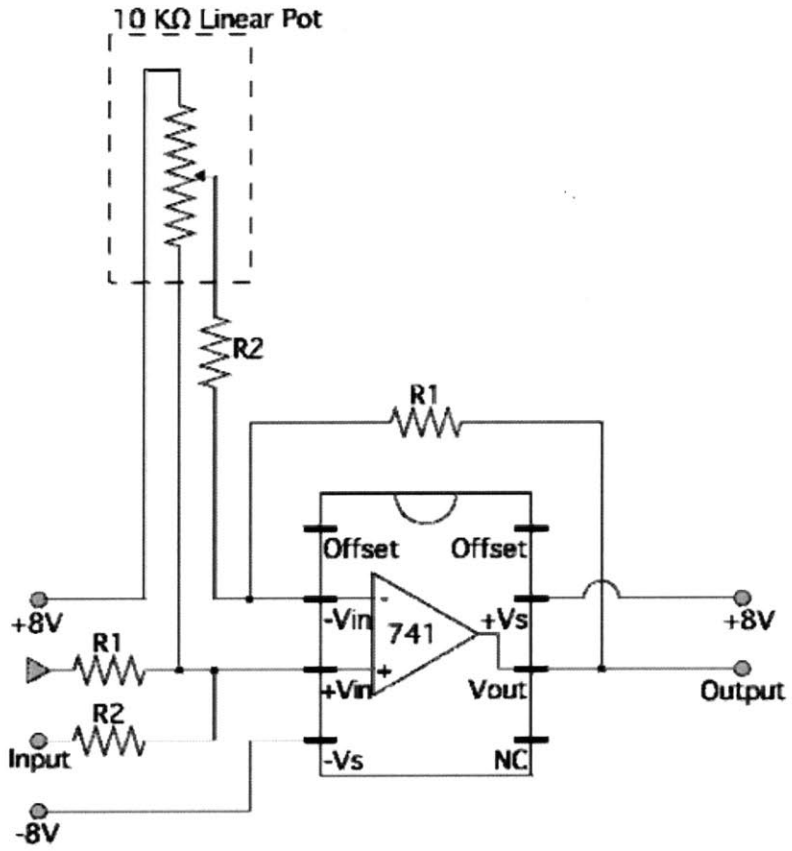

Figure 18. The circuit running the linear motors is a simple 741 subtraction circuit for proportional feedback control. The resistor values are picked such that a Kp of 30 is achieved (Reproduced from Daniel Cunningham SB2007).

An exceptional challenge was fitting the required power amplifier, wiring, and connectors into a package that could be integrated with the design of the actuator itself. A cylindrical aluminum housing was machined that contains the power amplifier and wiring. This cylinder mated with the back end of the actuator core to maintain a uniform cylindrical geometry for the entire package. The electrical connectors for power and signal input were installed in the back of the aluminum housing, enabling close-packing of the actuators even when fully connected.

In the following CAD model, the housing can be seen on the back, bolted to the cutaway view of Iteration 13.

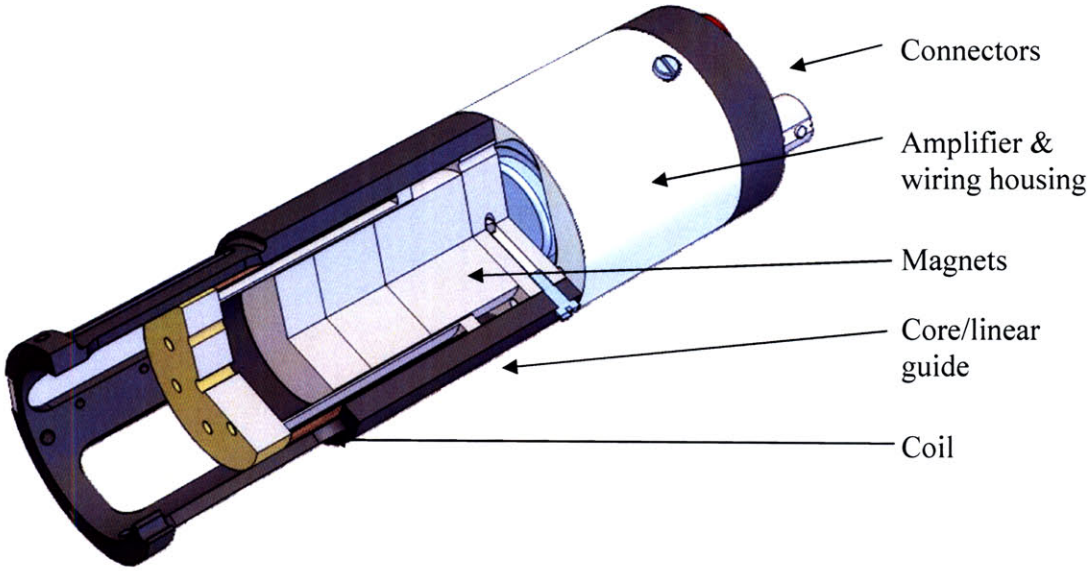

Figure 19. The amplifier and wiring housing can be seen at back, with the power amplifier nested into the aluminum on the front face. The cutaway view of the motor also shows stacked magnets in the core, bottom plate insert, field guide at the top of the core, and of course the coil itself and the forward-extended core that then serves as the linear bearing.

3.7 Actuator Packs

Once the actuators of Design Iteration 13 had been constructed with the control circuitry in the back, it was necessary to assemble them into a pack similar to that of the hobby servos from the original biorobotic fish fin. The objective was to create a modular pack of 5 actuators that could easily replace the original servos, and quickly and easily provide the increased functionality enabled by the LLAs.

The pack was constructed, and also filled the following functional requirements:

- Interface with original biorobotic fin design
- Each actuator can pull one tendon with forward motion and a second tendon with backward motion
- Interface with original frictionless sled design

3.7.1 Curl-Specific Design

The five-pack of actuators was built to test a curl-specific design of biorobotic fin. Of the four primary actuation modes in the pectoral fin's movement, the curl requires the most finesse and attention to replicate. As stated earlier, the Bluegill Sunfish's notable ability to produce forward thrust even on the recovery stroke of the pectoral fins adds a great degree of agility and maneuverability. In creating a biomimetic propulsion system with the same functionality as the Bluegill, it is critical to capture this functionality. A close-up of the cupping-specific design is shown below. As opposed to the urethane molded versions from the past, a very specific cupping pattern was desired, and thus rigid joint attachments were used, actuated by the LLA pack. Spandex material was sewn together to create the fin surface, which provided a favorable mix of compliance and hydrodynamic action when operating.

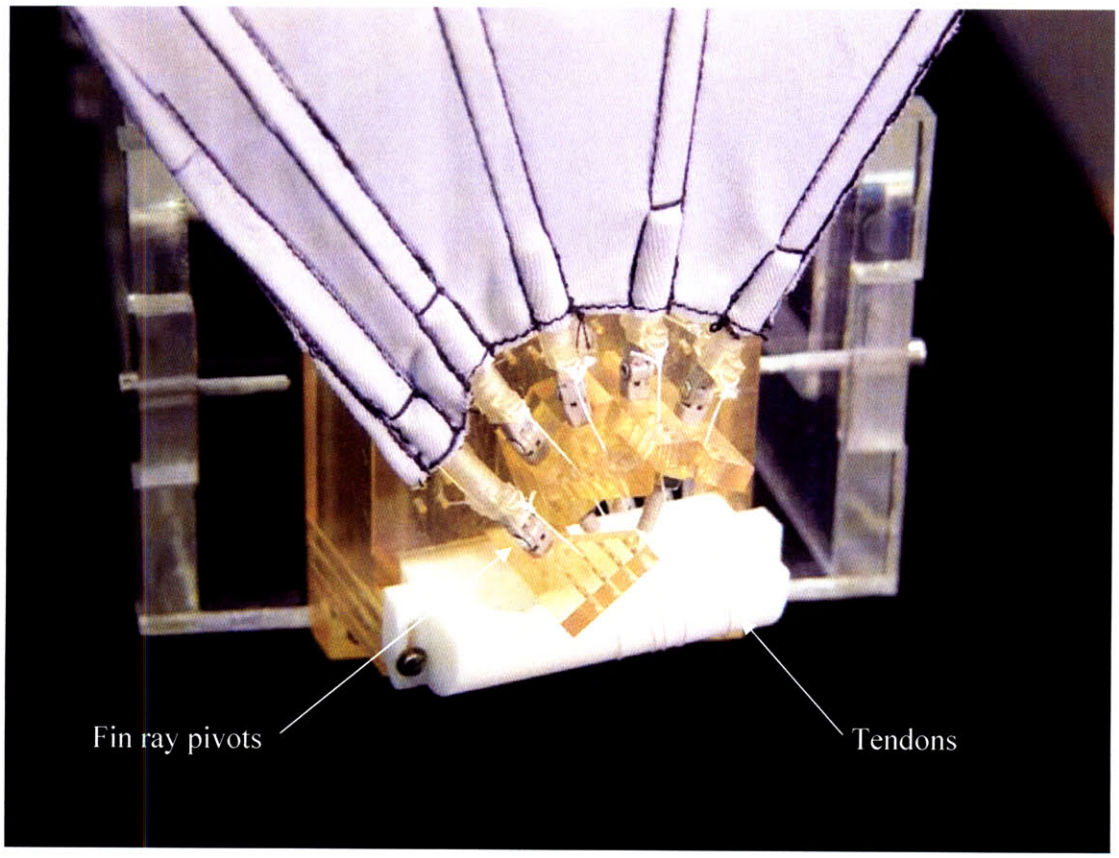

Figure 20. Rigid joints are used to confine the motion of the fin rays into a cupping-specific motion. The tendons wrap around the Teflon bar that acts as a pulley, and extend upward to the LLA pack (Photo by James Tangorra).

3.7.2 Construction of a Five-Actuator Pack

Similar to the construction of the frictionless air bearing sled, the pack structure was primarily created out of acrylic, with MK support structures. To achieve bidirectional pulling with an actuator whose operation is by definition push/pull, a bar of Teflon was employed in front of the attachment point of each tendon to the motor. By running a continuous loop that wrapped around the bar, pushing in the forward direction actually pulled the looped string, thereby creating a pull/pull actuator exactly suited to acting as an artificial muscle. The pack of five actuators is shown below in Figure 21, with a curl-specific fin attached.

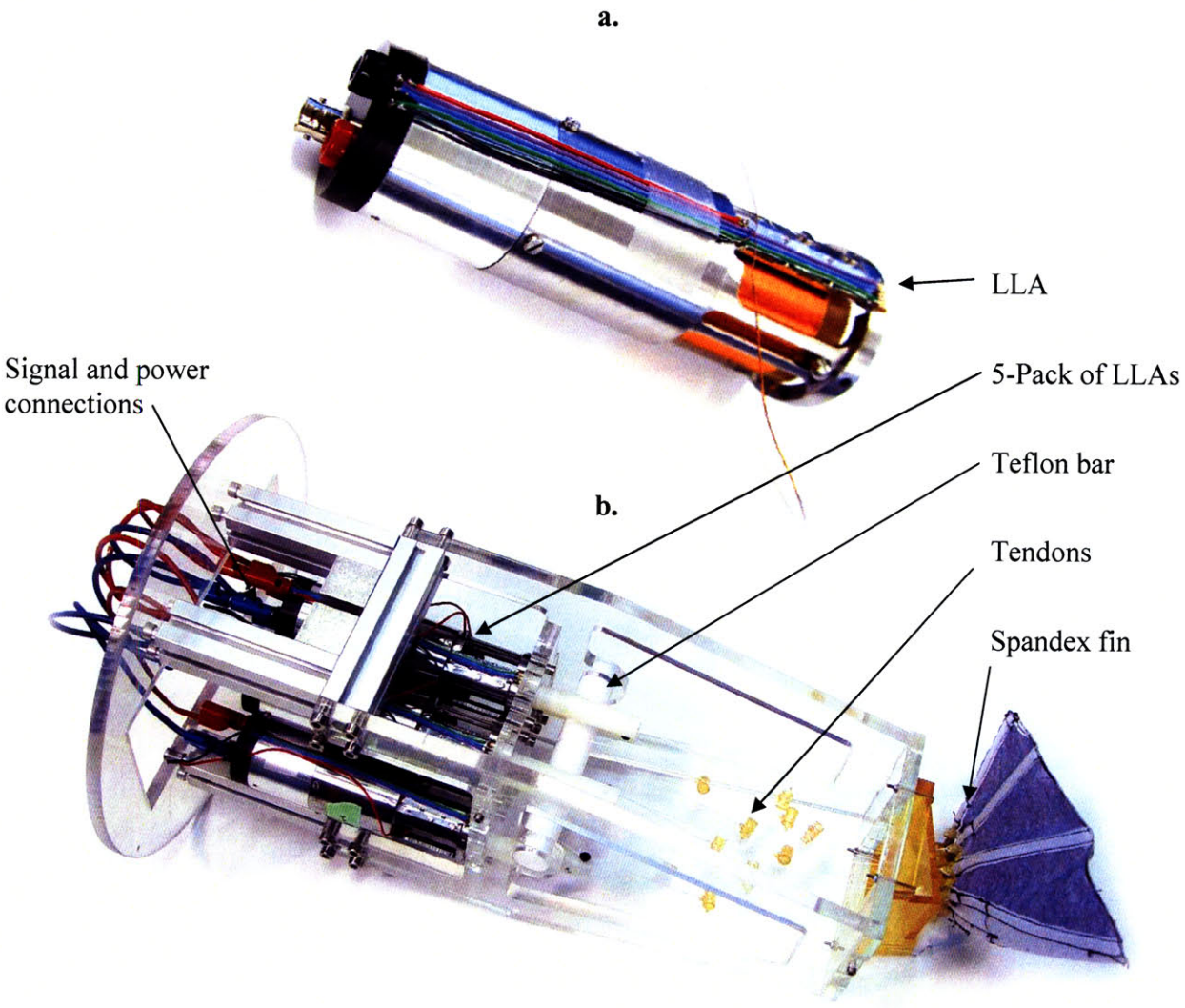

Figure 21a. Finished actuator with control circuitry, linear guide pin, and integrated position sensor. 21b. Actuator pack comprising five finished actuators, Teflon pulley-bar, tendons, and biorobotic fin for curl-specific testing.

3.7.3 Seven-Actuator Pack

After testing had been done with the five-pack of actuators, a more advanced version of the cupping-specific design was to be tested that also incorporated the expansion mode. For this purpose, the five-pack was upgraded to a seven-pack of actuators which also included current measurement of each motor, as well as a total current measurement of the whole pack. Hall-effect sensors were utilized in-line with the positive wire going to each coil, and the signal from the sensor was sent back to the data acquisition system. A break-out plate was constructed and placed on top of the seven-pack to more easily facilitate data input and output from the system, as well as hooking it up when inserting it and removing it from the flow tank.

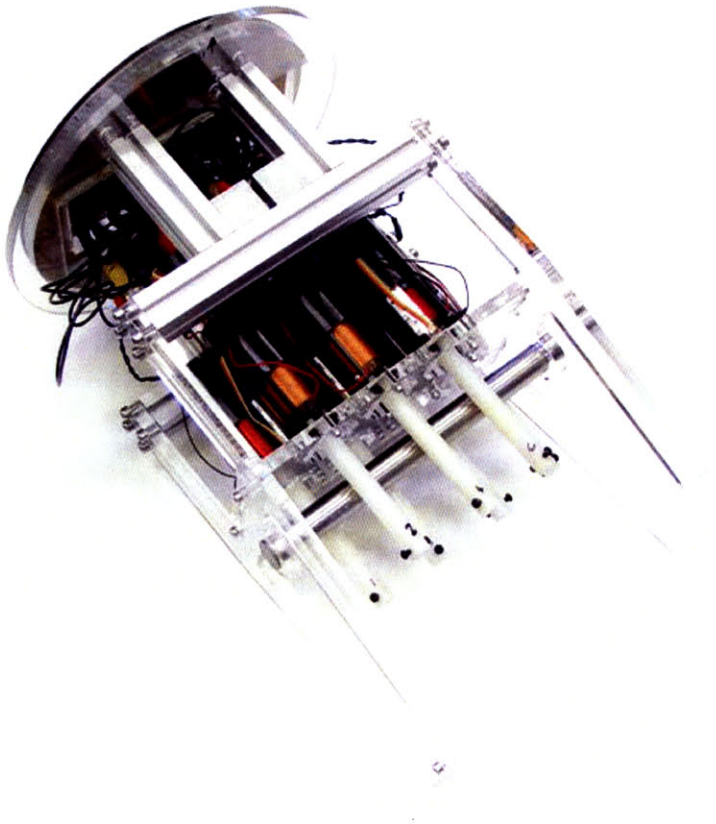

Figure 22. Seven-actuator pack. Tendons are wrapped around the smooth steel bar which then acts as a pulley, converting the push/pull force of the LLAs into a pull/pull configuration better suited to flexible tension members such as strings or tendons.

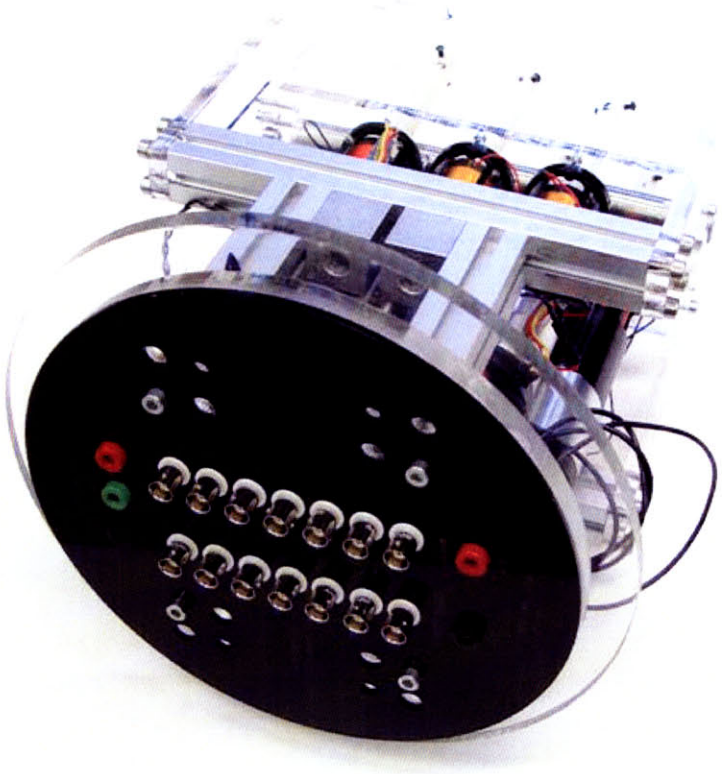

Figure 23. Seven-actuator pack with break-out plate on the front. Connections to the system are wired such that a user simply needs to plug into the needed BNC and power connections for full functionality.

3.8 Results of the LLAs in the Biorobotic Fin

Selected results of biorobotic fin tests are presented below in Figure 24 and Figure 25 These tests were conducted in a static flow tank on the air bearing sled whose design and construction is described in the previous chapter.

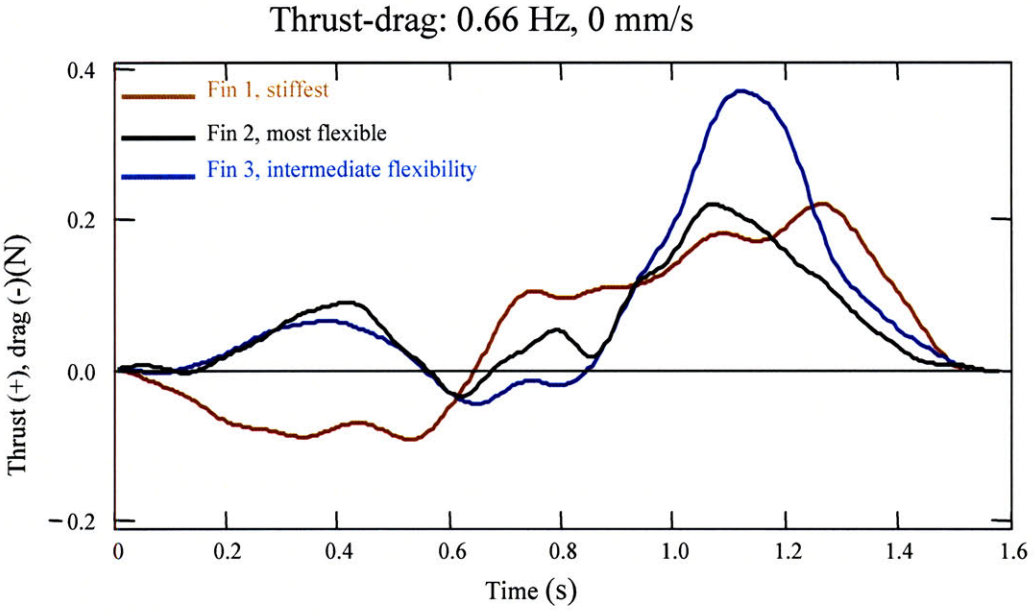

Figure 24 Thrust and Drag over time, comparison between different fin ray stiffnesses for isolated sweep mode (Data supplied by James Tangorra, January 12, 2007).

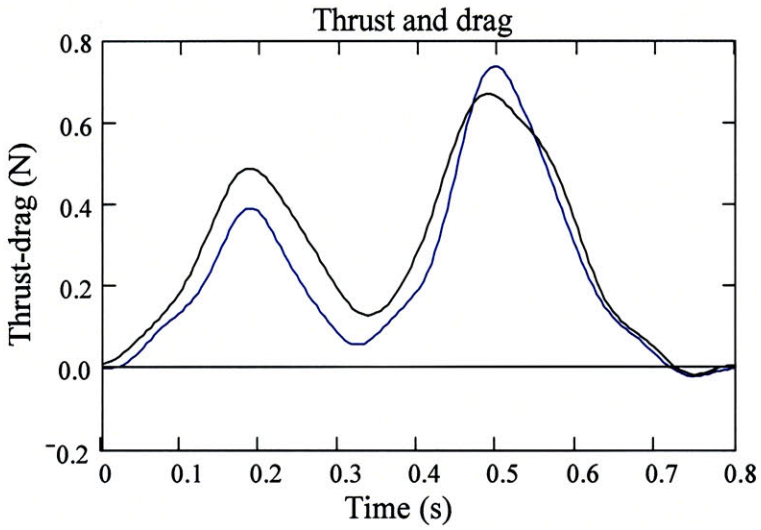

Figure 25. Thrust and Drag over time, on a 5-ray fin powered by a pack of LLAs under proportional position control. Cupping mode only. (Data supplied by James Tangorra, April 13, 2007).

3.9 Discussion

Figure 24 shows a comparison of three different fin ray stiffnesses during a test isolating the sweep mode of the fin. In the graph, thrust is positive on the Y axis, and drag is defined as negative force on the swimming body with relation to forward direction. It can be seen in Figure 24 that as the sweep progresses through time, the force appears as drag on the recovery stroke, and changes to thrust on the power stroke as the fin folds back toward the body.

Figure 25 shows the thrust-drag vs. time for a cupping-specific fin. It is the cupping mode that is responsible for the positive thrust during the recovery stroke, which can be seen clearly in the graph. The ability of the system to be easily fine-tuned for force and position output that was granted by the LLA pack enabled more rapid fin and testing iterations. The rapid iteration process was also aided by the easy reconfiguring of the actuator packs for the testing of the different fin designs.

4.0 Further AUV Applications – Final product

Beyond the biorobotic fish fin prototype, the actuators have use in other AUV systems. Two product-level actuators were created and shipped to the Office of Naval Research, where they are used in actuating a flex-fin style long range AUV system. These represented the final product of the biorobotic fin actuator development, and are shown in the figure below. These actuators are easily mass-producible and have broad applications in robotics and beyond.

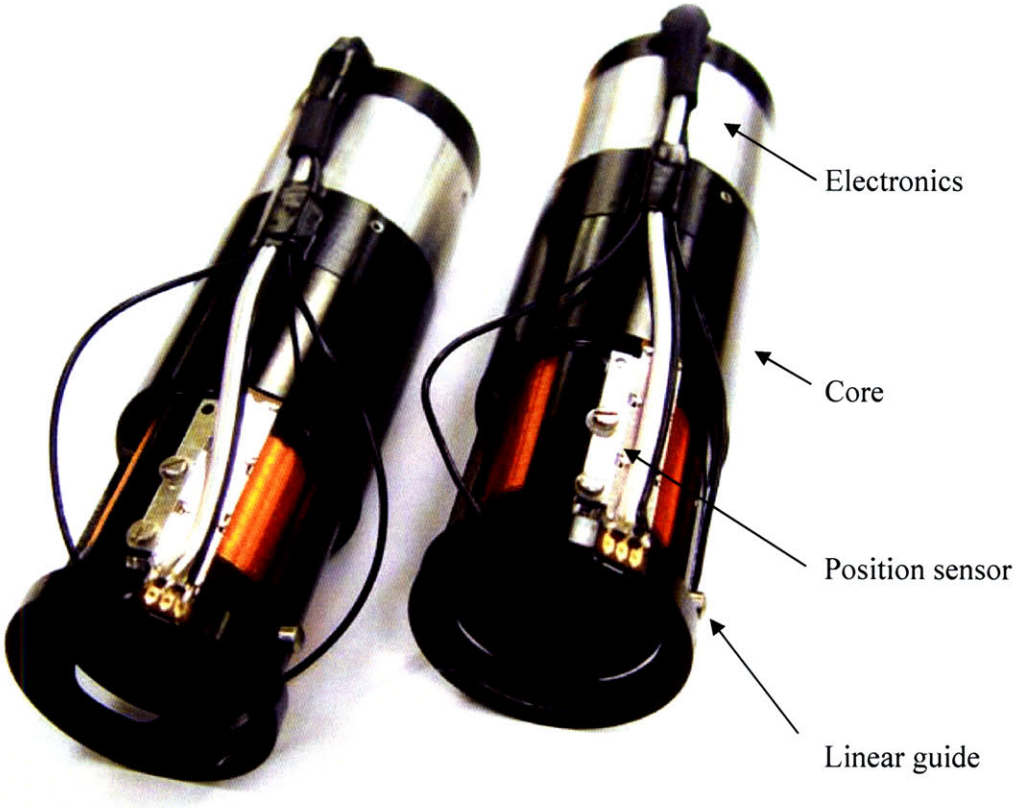

Figure 26. Iteration 14, the final product of the LLAs as designed for biorobotic applications.

5.0 Needle-Free Injection

Needle-free injection (NFI) has been in widespread use since the 1950s [14]. By developing high pressure (~20 MPa) behind a small-bore (~150 μm), a jet of fluid can reach sufficient velocity to penetrate skin. Traditional actuation methods to achieve the requisite pressures to accomplish this have included primarily high-pressure gas cylinders such as CO_2, and exceptionally strong springs [15], [16].

Though these methods are adequate to deliver a drug through the skin, there are limitations that continue to prevent their widespread use, as well as their maximum efficacy in delivering injections tailored to specific patient needs.

5.1 Benefits of NFI Use

Notable benefits exist with the use of NFI technology for drug delivery, including:

- Improved immune response [17]

  The even subcutaneous spread of drug through the tissue stimulates an improved drug uptake over traditional needle injections.

- Rapid injections

  NFI technology is ideally suited for mass-vaccinations. It is this technology that helped efforts to eradicate Polio [18].

- Reduced pain [20]

  When jet velocity approaches or exceeds 200 m/s, the skin's interpretation of the injection as pain significantly decreases.

- Reduced needle-stick injures for workers

  Approximately 59% of percutaneous injuries in health care workers are due to needles [19]. Use of NFI technology would potentially eliminate this risk completely.

- Reduced fear of injection

  Trypanophobia, or phobia of needles, affects many people. NFI systems can alleviate both this condition, as well as the general anxiety surrounding needle injections for both children and adults.

5.2 Existing Technology

Due to the low but non-negligible risk of cross-contamination of blood, and thus potential Hepatitis B transfer, the World Health Organization and the US Military—the two traditionally dominant users of NFI technology—have discontinued the use of NFI drug delivery, particularly in the form of Multi-Use Nozzle Jet Injectors (MUNJIs) [20]. Additionally, the CDC has recommended that NFI technology not be used for mass vaccinations unless the exceptional situation arises where the need outweighs the risk, such as in a bio-terror attack [20]. Thus, the main focus of NFI technology development is centered on consumer use where frequent personal injections are needed—such as with diabetic patients and in animal husbandry—where there is less concern over cross-contamination.

5.2.1 Limitations

Examining the two most prevalent NFI technologies: spring-actuated systems and gas-actuated devices, we find that significant performance enhancements can be achieved by upgrading the actuation system [11]. The focus of this section of work will explore the benefits that can be afforded NFI based on a fully controllable, low-cost actuator to drive needle-free injections. Though other needle-free technology exists that fires powdered drugs through the skin, we focused our efforts on examining fluid delivery devices for direct comparison to the systems we have created.

5.2.1.1 Spring-Powered Injectors

Several spring-powered injectors are on the market as consumer products, and are primarily directed toward diabetic users. These systems typically comprise a stiff spring, a screw or lever-type cocking mechanism, release mechanism, and some type of interchangeable syringe or drug ampoule. Examples are shown below in Figure 27.

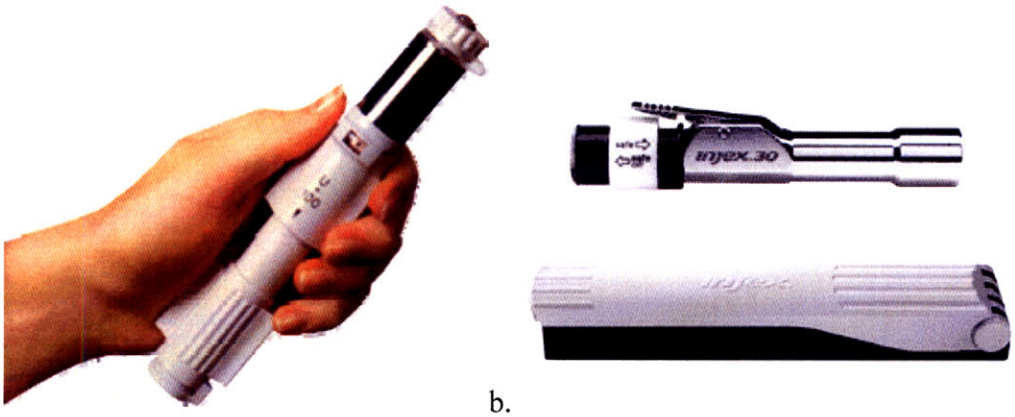

a. b.

Figure 27a. AdvantaJet NFI system (from advantajet.com) 27b. Injex injector sans syringe, with cocking mechanism below (from injex.com).

The primary limitation associated with spring-powered jet injectors within their intended application is controllability. Evidence suggests that varying the time-pressure profile of an injection can improve the performance of an injection [21]. The time-varying pressure profile of a spring powered injection is uniform, and the injection can only be modified from person to person by adjusting the spring preload prior to drug delivery. Devices constructed around spring actuation systems can sometimes be fine-tuned to achieve improved injection performance for a given individual, but that tuning is neither scalable from one person to the next in any rapid fashion, nor is it easy to select without a large number of trial-and-error injections.

5.2.1.2 Gas-Powered Injectors

Gas powered needle-free injectors, and specifically the type known as Multi-Use Nozzle Jet Injectors, maintain one of the biggest benefits of NFI technology, which is rapid sequential injections for multiple patients [20]. It is partly for this reason that the technology is so clearly beneficial for military, humanitarian, and emergency use. A famous picture of a jet injector in use is shown below for reference. The device in use is the Ped-O-Jet, which reached the height of use in the 1970s to 1980s. It is the most widely distributed and used jet injector system in existence.

Figure 28. The Ped-O-Jet in use. Note the amount of force necessary to hold the jet against the patient's arm. The Ped-O-Jet was known for 'slicing' tissue if it was not held tightly enough to the arm during an injection (Photo from Centers for Disease Control, www.cdc.gov).

The same controllability limitation is present in gas powered injectors. Though a very limited capability exists to fine-tune an injection profile over time in a gas injector, in the case of rapid fire injections the capability is rendered unusable. The device will be effectively administering the same injection to each and every person down the line, whether the patient is a 6 year old child or a tough-skinned man in his prime.

Clearly, it is not desirable to administer the same shot to a child that was just administered to fully grown man, or vice versa. The child's shot would not penetrate deep enough for the adult, and the adult's shot would go into the muscle of the child. There is thus a strong impetus from both consumer and humanitarian standpoints to develop a fully portable needle-free injection system with controllable time-pressure profiles that can quickly and easily tailor optimized shots to a wide range of patients.

5.2.2 Prior Work in the MIT BioInstrumentation Lab

Extensive work has already been performed in the BioInstrumentation lab on fully controllable NFI devices [11], [22]. Using a large, high-power LLA to drive needle-free injections into post mortem guinea pig tissue as well as in-vivo lamb skin, we have already determined the benefits of delivering injections via varying time-pressure profiles [11], [22], [23], [24]. A picture of the large-scale LLA-powered NFI system in use is shown below.

Figure 29. The Bioinstrumentation Lab LLA powered NFI prototype in use on a sedated sheep (Reproduced from Brian Hemond SM2005).

This prototype worked well and proved the concept's feasibility, but was also bulky and difficult to maneuver while performing injections, as can be seen in Figure 29. Despite the obvious advantages of controllable injection profiles, for such needle free injection devices to become ubiquitous, they must be small, portable, and inexpensive while maintaining their functionality [11].

Miniaturizing the technology necessary to successfully drive injections via an LLA device is a clear challenge with significant benefit. Additionally, with the advent of a truly handheld device with adequate power to carry off multiple needle-free injections in a row, a new breed of higher volume NFI devices could open up that use multiple injections each to sustain controllable high pressures for longer injection times.

5.2.3 Adaptation of the Biorobotic LLA for NFI Use

The exceptionally high performance of the LLA developed for the biorobotic fish fin is attractive to many other applications. In particular, its high force constant enables it to produce much more force than its commercially available counterparts, making it especially well-suited to a high power NFI application where other actuators would not. Its built-in linear guide also makes it well-suited to easy integration in other systems, such as a handheld NFI device.

The new LLA is roughly one-quarter the mass of the original voice coil that runs the older NFI prototype, but has half the force constant at 11 N/A. The key to making such a small system work effectively without burning out the coil is using the coil with a low duty cycle. Because the thermal time constant of the coil and motor assembly is so much longer than the Joule heating impulse produced by 100 ms pulse of 20 A, over-driving the 0.35 mm diameter wire (28 AWG) in the coil does not produce a risk of overheating.

5.2.4 Implementation of the LLA in the NFI

Using a stereolithography apparatus (SLA) for 3D printing, a housing was constructed to hold the LLA. A new front plate was fabricated to accommodate the off-the-shelf Injex syringes, which are M8 threaded in their attachment. The front of the coil was tapped for an M3 thread, and a matching M3 was threaded onto the back of the piston. The diagram below in Figure 30 illustrates the configuration of the clinical version of the device.

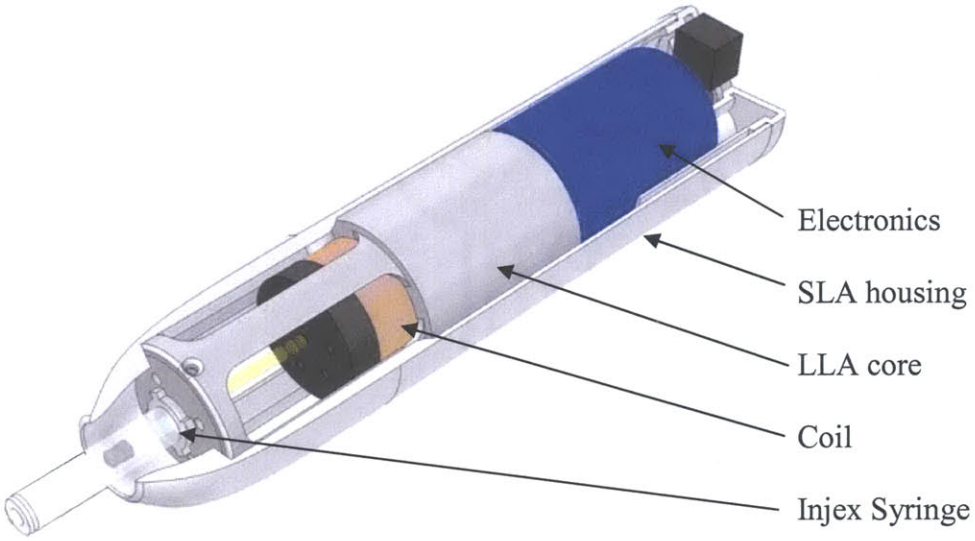

Figure 30. The clinical handheld NFI prototype, with LLA, coil, syringe, and plunger all visible.

For the research version of the hand-held NFI, an AE-Techron LV5050 power amplifier is used to power the system. Using LabView, the time-varying injections can be servoed off of position, velocity, current, or pressure.

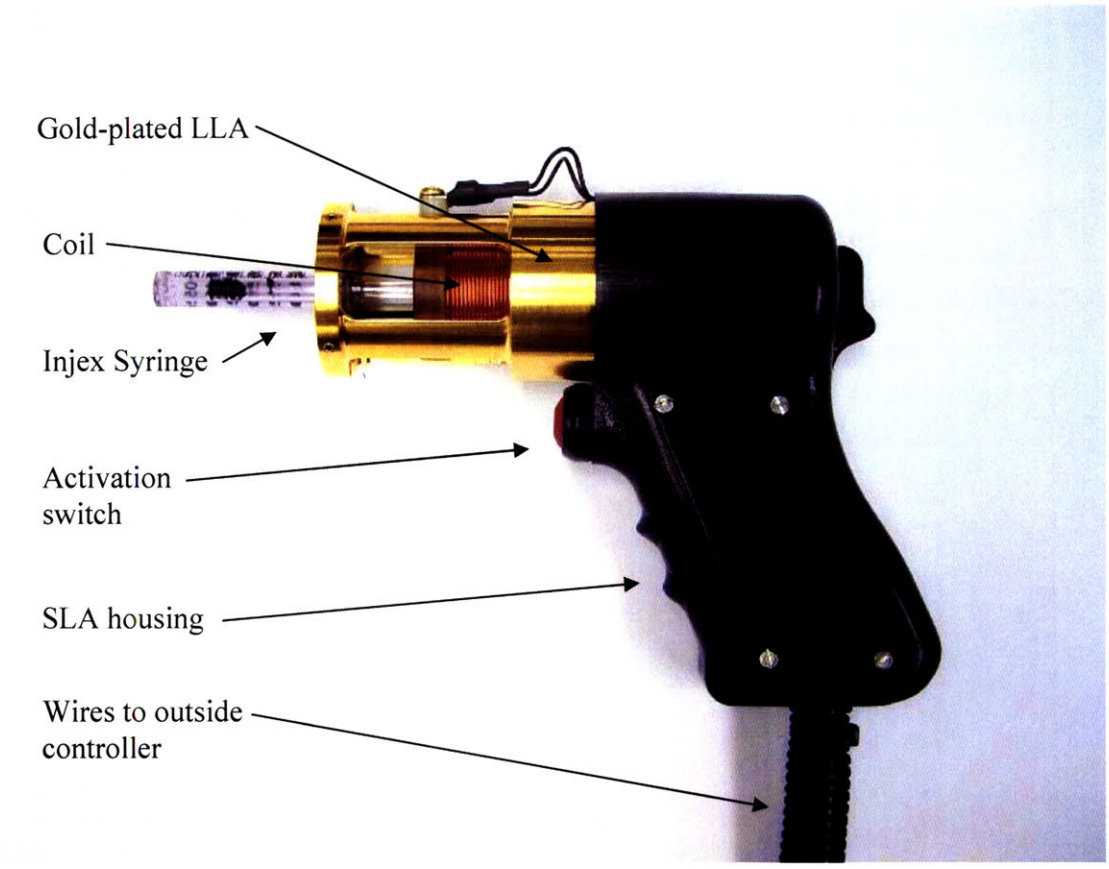

Figure 31. Hand-held NFI for research use. The gold coating prevents corrosion of the steel casing. Flexible leads attach the coil to the system. The trigger button fires, and Injex OEM syringes screw into the M8 threads at the front of the device. Power, control, and electronics are outside the system.

5.2.5 Results of Improved LLA Implementation in NFI Device

In the following figures, various injection performances are recorded for both off-the-shelf NFI systems and the LLA-powered NFI device shown in Figure 31, as denoted in the figure captions.

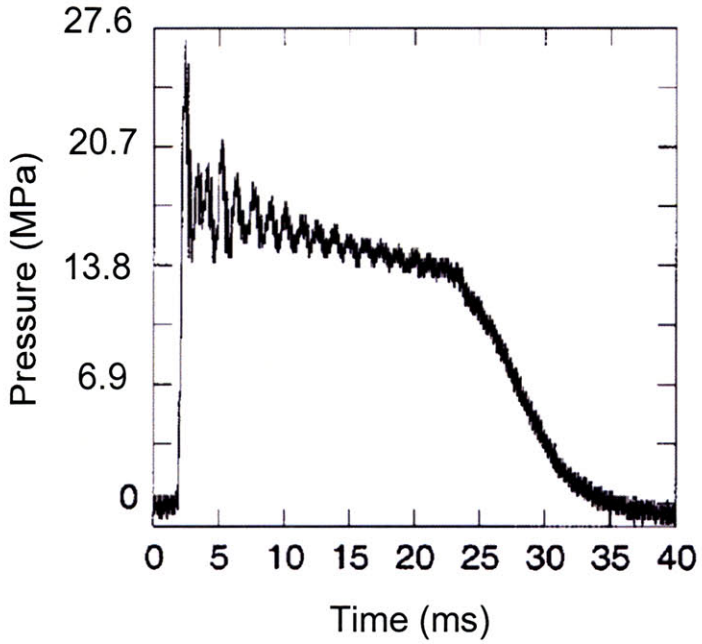

Figure 32. Pressure vs. time of a commercial needle-free injector (Adapted from Schramm-Baxter, 2004).

In the figure above, the pressure profile of a spring-powered injection can be seen. This injection profile will be constant from one delivery to the next, and is not tunable between patients. Though the pressure is comparable to that of the LLA-powered NFI delivery, significant second-order resonance can be seen in the follow-through of the injection. Figure 33 shows the step response of the LLA-powered needle-free injector that is shown in Figure 31 Note that the second-order resonance is significantly decreased. This profile is fully tunable through time, and can be varied by running the pressure, velocity, or position on feedback control.

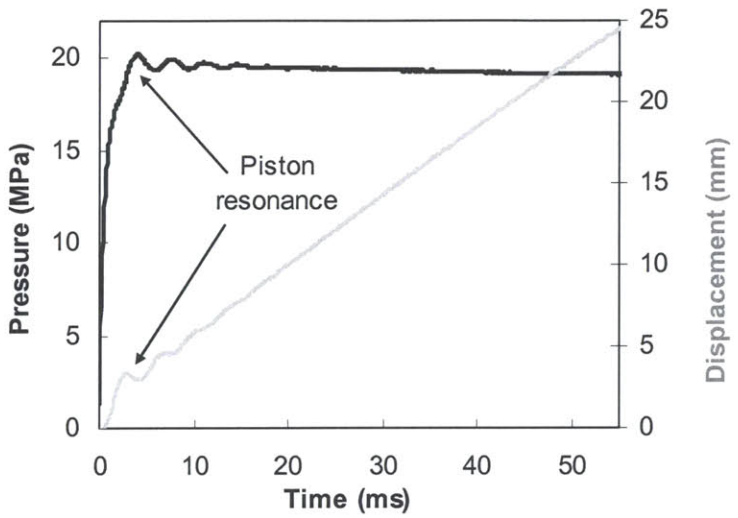

Figure 33. Single forward shot of LLA-powered needle-free injector. Input is a step function (Reproduced from Taberner et al, 2006).

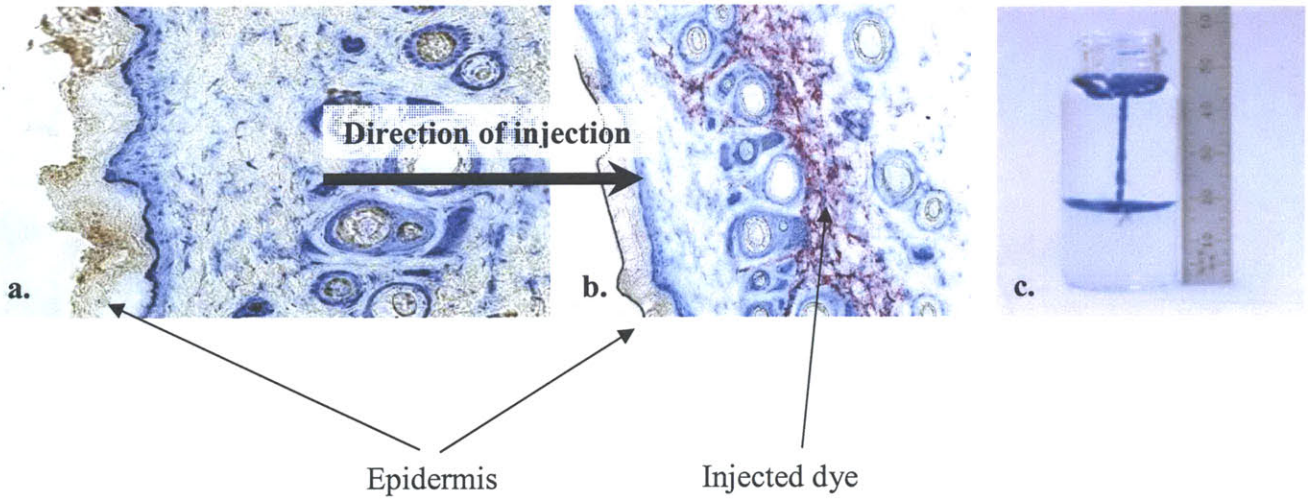

Figure 34a. Injection of purple dye into dermis via needle-free handheld system. 34b. Dye post-injection. 34c. Test injection into acrylamide gel (Reproduced from Taberner et al, 2006).

Figure 34 above shows a needle-free injection of dye into post-mortem guinea pig tissue. The lateral distribution of the purple dye below the skin can be seen in the transverse cut. The far right of the figure demonstrates the same subcutaneous spread in acrylamide gel which is formulated to simulate flesh. By controlling the velocity of the outgoing jet, injection depth can be accurately varied from 5 mm to 22 mm depths with the LLA-powered system described above. This demonstrates the flexibility necessary to carry off

injections of the same depth for a given drug for many different skin types and thicknesses. This is an advantage that only controllable actuators can grant NFI systems.

6.0 Rapid Fire High-Volume NFI System

The ability to control pressure-time profiles for needle-free injections is beneficial over any time duration of injection. The aforementioned systems were designed around existing needle-free syringes whose maximum dose is 250 μL. For larger injections, either the size of the syringe itself must be increased, requiring a longer-travel LLA, or the diameter of the syringe must increase, requiring higher force output from the actuator. To maintain a compact size of NFI drug delivery device, it is advantageous to use two small, optimized LLAs in reciprocating fashion, such that one is filling a drug cylinder while the other is firing it. A schematic diagram is shown below in Figure 35 which depicts a two cylinder NFI device designed to deliver up to 2 mL/second.

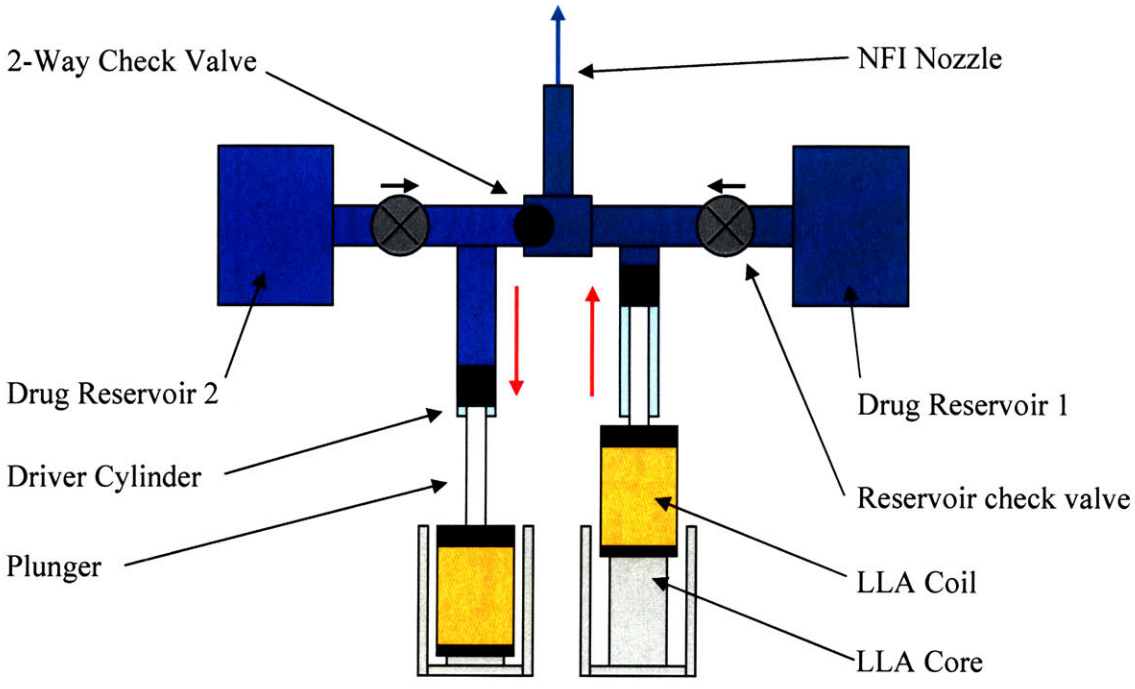

Figure 35. Schematic of Rapid Fire High Volume NFI System

6.1.1 Rapid Fire NFI Principles of Operation

The operation of the rapid fire NFI system is based off of a reciprocating pump. Check valves direct the drug flow from each reservoir forward to the injection nozzle. Pressure is generated by the forward motion of each LLA. With a 180° phase shift, one side will be filling its driver cylinder while the other is firing. In this configuration the volumetric flow rate is only limited by the power input to the system, and how much continuous power each coil can take without overheating. The system was designed to drive 2 mL/second continuous at 3 MPa, which achieves the baseline performance necessary to perform high-volume needle-assisted injections, which have a lower pressure requirement than do needle-free injections. Scaling the system to higher pressures such as 10-20 MPa for true needle-free injections is simple, only requiring more power input at a lower duty cycle for the same rapid fire device.

6.1.2 Two-Way Check Valve

In the model depicted in Figure 35, a specialized check valve design is incorporated that combines two check valves into one. The ball seen in the middle is constrained within its chamber, and has inverse conical seats on each side where it can make a seal. The left side is filling while the right side is firing. The filling pressure is lower than atmospheric, such that drug will be drawn from the left reservoir through the reservoir check valve and into the driver cylinder as the left coil moves backward.

Similarly, the pressure on the right side of the system is dramatically increased from the forward force provided by the LLA on the right side. The resulting pressure differential between the left and right sides of the rapid fire system pulls the floating ball into the seat on the left side, enabling a sealed fill on the left, and a sealed injection for the right side. A prototype of this system is shown below in Figure 36

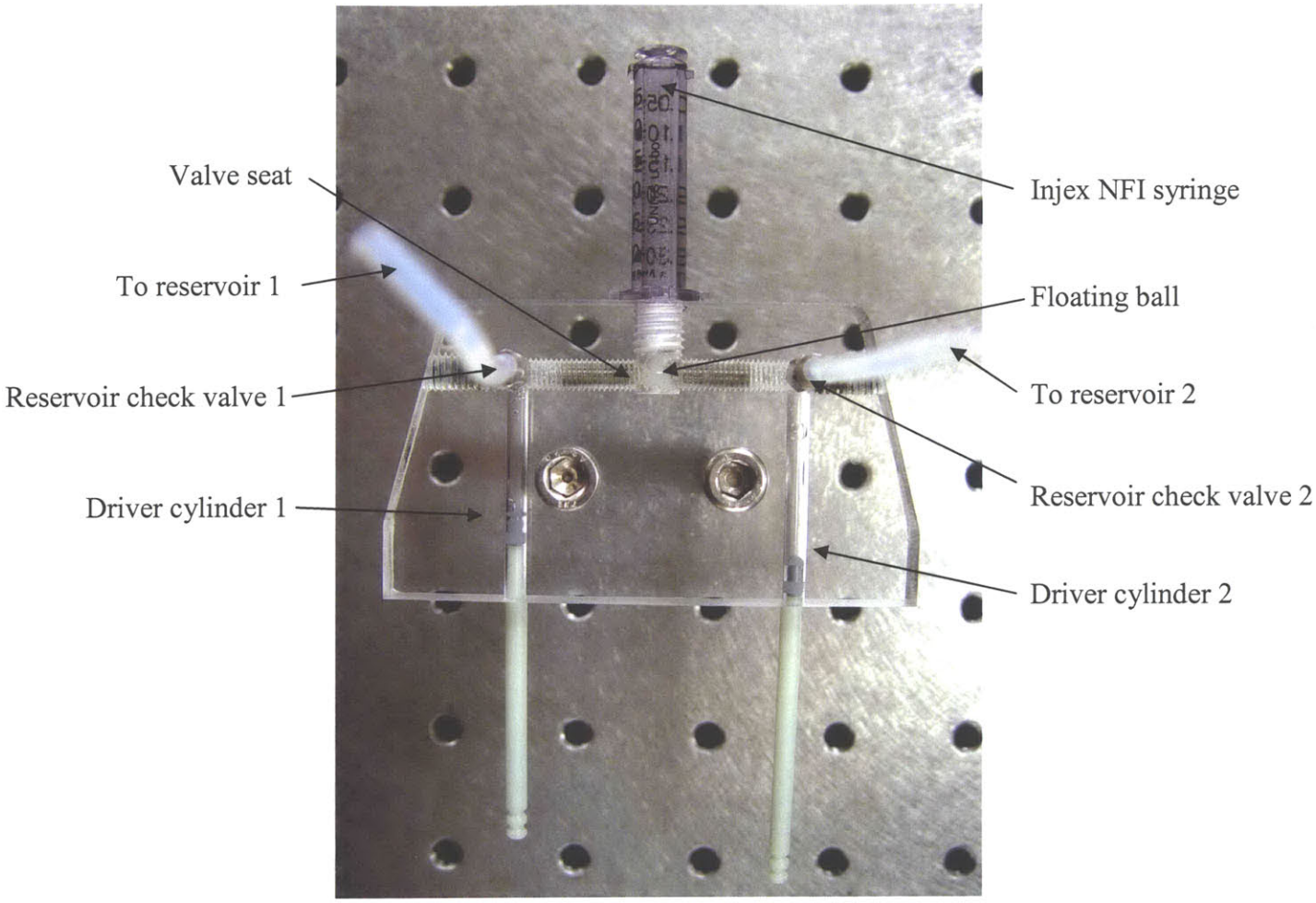

Figure 36. Bench-level prototype of rapid fire device. Main body is constructed from acrylic. Piston cylinders are drilled and reamed.

The prototype's success indicated that the system, and most importantly the check valve, would function at least as a reciprocating pump. A key component of the desired success was that positive pressure be maintained across LLA reciprocations in order to create an uninterrupted injection. To test full functionality of the device, a full scale mockup was created that used LLAs under position feedback control in order to test different input waveforms. The intent was to determine if the custom check valve was capable of passively moderating flow between the two driving sides, and if the pressure could be maintained above zero. The bench top test system is shown below in Figure 37.

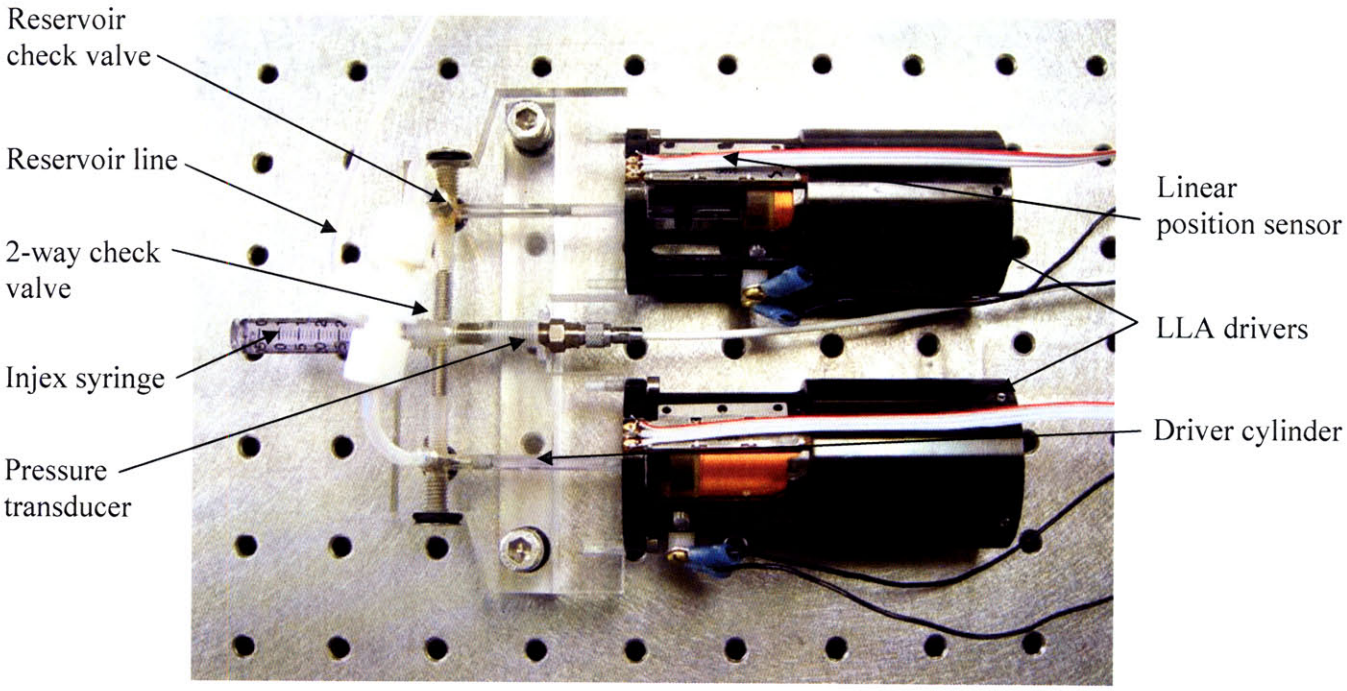

Figure 37. Bench top test system of rapid-fire NFI. LLAs power each side under position feedback control.

6.1.3 Rapid Fire Iteration 1 Testing

The system showed promise, but from the pressure data collected it is clear that the two-way check valve cannot maintain positive pressure in-between LLA cycles. It is clear that by simply running square waves that are 180° offset, there will be a dead zone during the transition between filling and firing for each side. During this instant, pressure in the system will drop to zero at the point when the LLAs are changing direction. This was verified experimentally. The proposed solution was to keep the waveforms offset, but to drive the LLAs under position control to follow asymmetric sawtooth trajectories. By managing the sawtooth timing so that at least one actuator was driving forward at all times, the hope was that positive pressure could be maintained. The driving waveform and resulting pressure are shown below.

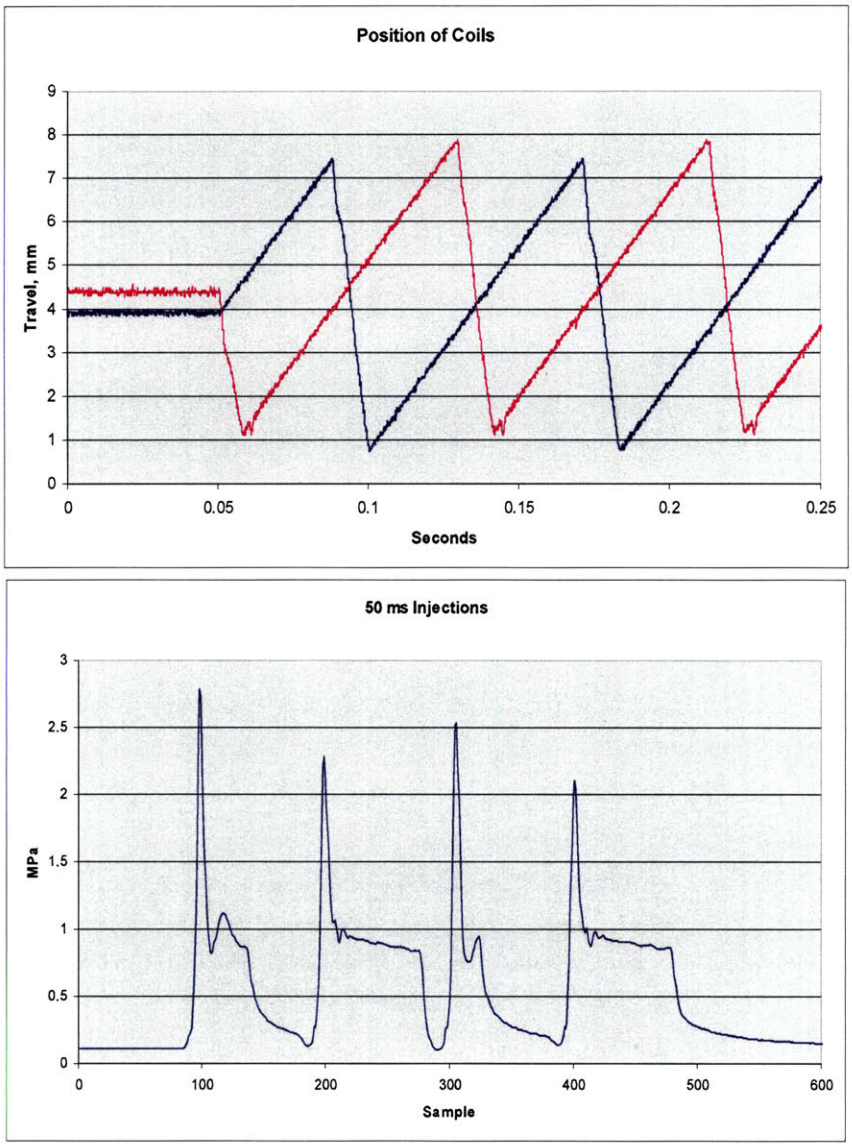

Figure 38. Driving waveform (top) and resulting pressure output of rapid fire NFI prototype (bottom).

As can be seen from the figure, the waveforms were at 90% of the maximum retracting speed, which gave as much time as possible to forward driving. Observing the pressure profile in the lower portion of Figure 38, the pressure still drops to zero during the transitions. This was attributed to the momentary pressure equalization that occurs in the two-way check valve each time an LLA reverses. The solution was to do away with the custom valve, and resort to a full set of four single side check valves.

6.2 Rapid Fire NFI System with Four Check Valves

The system was reconfigured with the switch to classic check valves. Because air in the system decreases output pressure and risks potentially fatal injections of air into the bloodstream, the system was rotated upright to ease the bleeding of air bubbles. The new test setup is shown below.

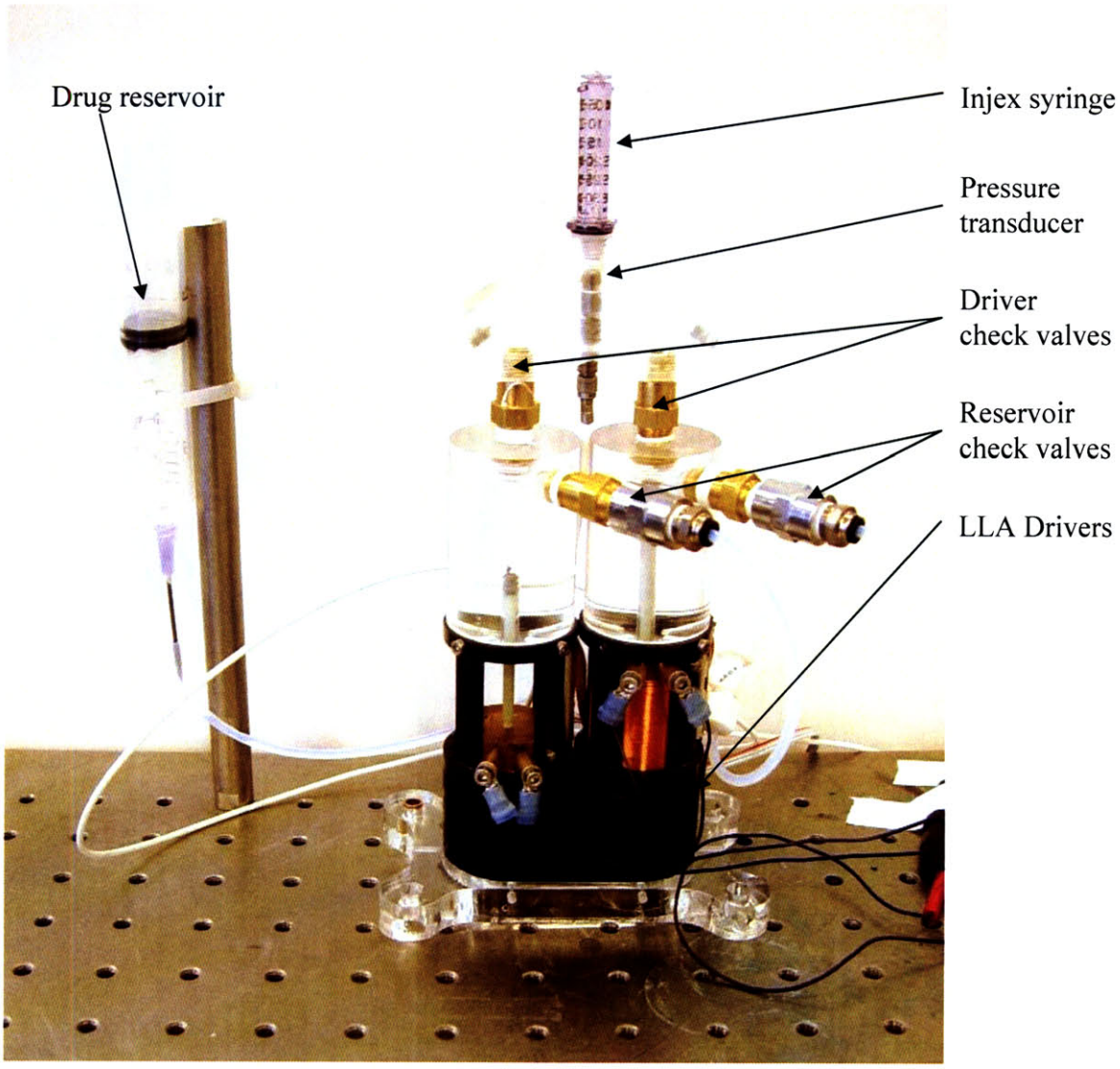

Figure 39. Rapid fire NFI setup with four check valves. System is rotated upright to enhance air bleeding.

6.3 Check Valve System Results

The change to standard check valves resulted in a significant performance increase, both in continuous positive system pressure and in peak pressure. The data are presented below in Figure 40.

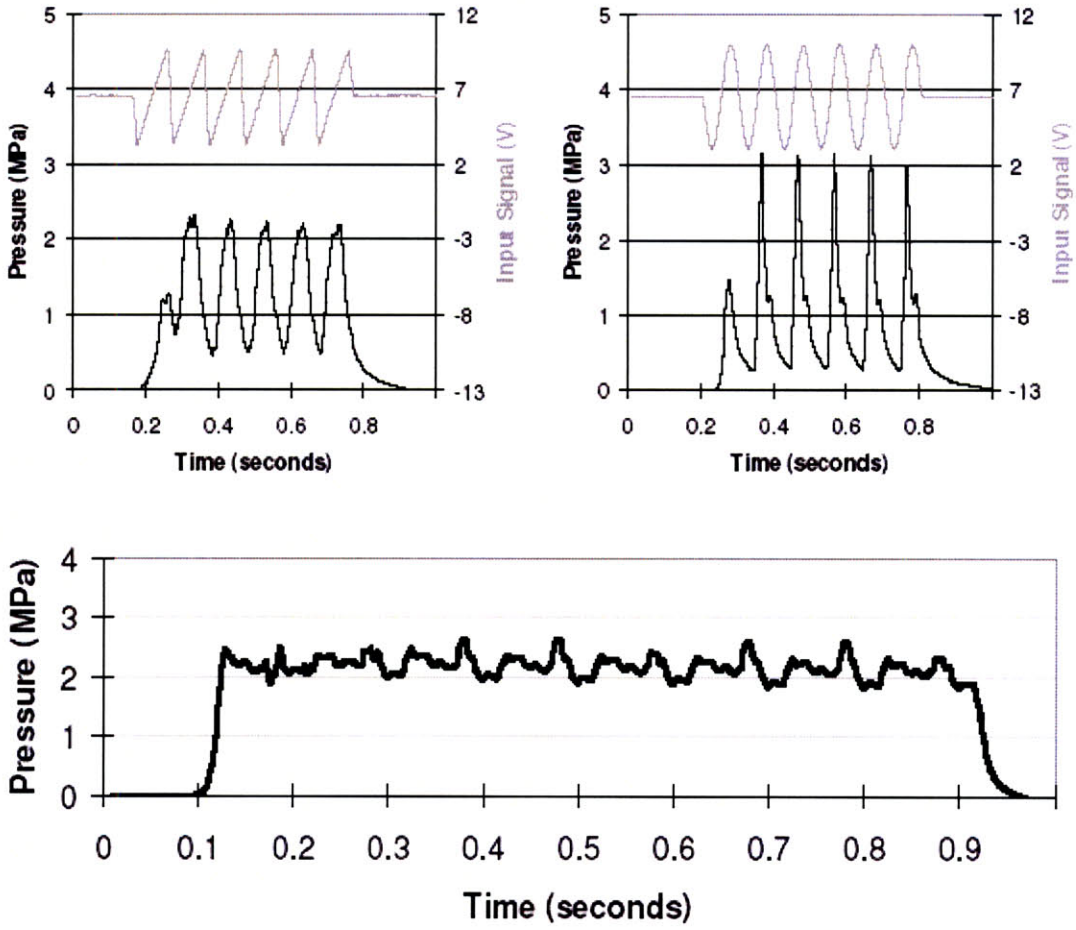

Figure 40. Results of testing check valve system. Top left: single-side test with sawtooth wave input. Top right: single-side test with sinusoid input. Bottom: 8-cycle burst with both LLAs driving 180° offset (Reproduced from Daniel Cunningham SB2007).

6.4 Check Valve System Discussion and Implications

The results from Figure 40 show that the system was capable of producing its intended sustained pressure of greater than 2 MPa for the duration of a cycle. This base level functionality is sufficient for even the existing system to be reproduced and immediately applied to needle-assisted drug delivery systems, and would only require a higher power electronic driving system to achieve greater pressures. By scaling up the power supply, sustained pressures of up to 20 MPa could easily be achieved in order to drive true high volume needle-free drug deliveries.

7.0 Conclusions and Recommendations

The optimized Linear Lorentz-force Actuator that has been developed and documented in this thesis has a broad range of applications, and can enhance the functionality of many systems and devices beyond the scope of this thesis. The compact size and low mass makes it especially suitable for biorobotic applications such as the robotic fish fin described in this work, and also for high power compact systems like the NFI.

The potential benefits of using the improved LLA in a biorobotic fish-inspired AUV are notable, as previously discussed. Increased controllability, stealth, efficiency, and thrust output of the biorobotic fin prototype were verified by test results, and could be immediately implemented in a working AUV prototype. For applications requiring paramount maneuverability and stealth, such as searching for underwater mines in a hostile marina or autonomous ship hull inspection, a biorobotic fin such as that described in this thesis would provide an effective and easily utilized solution for such underwater maneuvering.

The implications of the LLA's application in needle-free injection devices are even more significant. Because of their inherent controllability, benefits beyond customized time-pressure injection profiles can be immediately reaped. The primary factor contributing to the cross-contamination risk of Hepatitis B when using MUNJI devices is blood backflow

into the NFI nozzle. During an injection, a small fluid packet often remains in the dermis before the drug is fully absorbed. As the pressure from the incoming jet decreases at the end of the injection, the fluid packet can squirt a small amount of blood back into the injector's nozzle [20]. Using a controllable actuator such as the LLA described in this thesis, the pressure at the end of the injection can be shaped to spike as the NFI device is removed from the skin, thus decreasing the blood backflow into the nozzle.

In the best-case scenario, an LLA-actuated NFI device could eliminate the cross-contamination risk to a degree that the CDC and WHO would resume use of the technology for routine mass-injections around the world. Additionally, its widespread use could bring optimized injections of any volume to patients, in both domestically and in the third world, at lower cost, greater throughput, and with less pain.

Future work on these devices that would enhance their benefit even further would be the integration of a self-optimizing digital controller and driver such as that developed by the MIT BioInstrumentation Laboratory. As opposed to the classical feedback control implemented in this thesis, the self-optimizing controller can re-tune its parameters in real time to greatly improve performance in any use scenario. The integration of this controller into the LLA and the subsequent packaging as a self-contained unit would be an extremely powerful product whose unparalleled performance would set a new precedent for compact high power precision actuators.

Finally, for NFI system use, a last advancement the voice coil technology enables is the dual use of the actuator as a true transducer. By pushing the NFI nozzle against the skin and pulsing the coil through a range of frequencies while measuring the force of the tip against the skin, a compliance model for the dermis itself can be determined via stochastic system identification techniques. This means that the NFI could test the skin mechanically and determine an optimized time-pressure profile for any given patient in a matter of seconds—and then immediately deliver that injection. Such a tool would truly enable rapid throughput, optimized injections of any volume: a capability never before realized in a portable device.

8.0 References

1. BEI Kimco Magnetics – 2470 Coral Street, Building D. Vista, CA 92081-8430

2. Meins, J. Miller, L. Mayer, W. J. The High Speed Maglev Transportation System Transrapid. *IEEE Transactions on Magnetics,* 24(2):808-811 1988.

3. Brückl, S. Feed-Drive System with a Permanent Magnet Linear Motor for Ultra Precision Machine Tools. *Proc. IEEE International Conference on Power Electronics and Drive Systems,* 2:821-826, 1999

4. Heyne, C. Electromagnetic Launcher with Powder Driven Projectile Insertion. US Patent 4,555,972

5. Tangorra, J. Davidson, S. Madden, P. Lauder, G. and Hunter, I. A Biorobotic Pectoral Fin for Autonomous Undersea Vehicles. *Proc. 28th IEEE Engineering in Medicine and Biology Society*, 2726-26729, 2006

6. Fish, F. E., Lauder, G. V., Mittal, R., Techet, A. H., Triantafyllou, M. S. Conceptual Design for the Construction of a Biorobotic AUV Based on Biological Hydrodynamics. *Proc. 13th Int. Symposium on Unmanned Untethered Submersible Technology,* 2003.

7. Lauder, G.V. Function of the Caudal Fin During Locomotion in Fishes: Kinematics, Flow Visualization, and Evolutionary Patterns. *American Zoologist,* 40:101-122, 2000

8. Gibb, A. C., Jayne, B. C., Lauder, G. V. Kinematics of Pectoral Fin Locomotion in the Bluegill Sunfish Lepomis Macrochirus. *Journal of Experimental Biology.* 189:133-161, 1994

9. Lauder G. V., Drucker, E. G. Morphology and Experimental Hydrodynamics of Fish Fin Control Surfaces. *Proc. 13th Int. Symposium on Unmanned Untethered Submersible Technology,* 2003

10. Madden J., Schmid B., Hechinger M., Lafontaine S., Madden P., Hover F., Kimball, R., Hunter I. Application of Polypyrrole Actuators: Feasibility of Variable Camber Foils. *IEEE Journal of Oceanic Engineering,* 29(3),738-749, 2004

11. Taberner, A. Ball, N. Hogan, C. Hunter, I. A Portable Needle-Free Jet Injector Based on a Custom High Power-density Voice-coil Actuator. *Proc. 28th IEEE Conference, Engineering in Medicine and Biology Society*, 5001-5004, 2006

12. Bozkurttas, M. Dong, H. Mittal, R. Madden, P. and Lauder, G. Hydrodynamic Performance of Deformable Fish Fins and Flapping Foils. *Proc. 44th AIAA Aerospace Sciences Meeting and Exhibit*, 1-11, 2006

13. Alps Electric (USA), Inc. Suite #500, 910 E. Hamilton Ave. Cambpbell, CA 95008.

14. Howard-Jones, "A Critical Study of the Origins and Early Development of Hypodermic Medication," *Journal of the History of Medicine and Allied Sciences*, 2:201-249, 1947.

15. Castellano, T. P. "Modular gas-pressured needle-less injector," U.S. Patent 6,613,010

16. Lilley, S.J. Taylor, H.F. Theobald, D.R. Carlson, C.J. Rosen, D. I.Medical Injection System and Method, Gas Spring Thereof and Launching Device Using Gas Spring, U.S. Patent 5,599,302

17. Gramzinski, R. A., Millan, C. L., Obaldia, N., Hoffman, S. L., and Davis, H. L. Immune response to a hepatitis B DNA vaccine in Aotus monkeys: a Comparison of Vaccine Formulation, Route, and Method of Administration. *Mol. Med.*, 4:109–118, 1998.

18. Hingson, R. Davis, H. Bloomfield, R. Brailey, R. Mass Inoculation of the Salk Polio Vaccine with the Multiple Dose Jet Injector. *GP,* 15(5):94-6, 1957

19. *CDC Sharps Safety Workbook,* Centers for Disease Control, Atlanta, Georgia, USA. www.cdc.gov.

20. Weniger, B. Jet Injection of Vaccines: Overview and Challenges for Mass Vaccination with Jet Injectors. *Proceedings: Innovative Administration Systems for Vaccines,* 2003.

21. Shergold, O.A. Fleck, N.A. King, T.S. The Penetration of a Soft Solid by a Liquid Jet, with Application to the Administration of a Needle-Free Injection, *J. Biomech.*, 39(14):2593-2602, 2006

22. Wendell, D.M. Hemond, B.D. Hogan, N.C. Taberner, A.J. Hunter, I.W. The Effect of Jet Parameters on Jet Injection, *Proc. 28th Annual Conference of the IEEE EMBS,*5005-5008, 2006

23. Wendell, D. Controllable Needle-Free Injection: Development and Verification of a Novel Device. Thesis for Master of Science, MIT, 2007

24. Hemond, B. A Lorentz-force Actuated Controllable Needle-free Drug Delivery System. Thesis for Master of Science, MIT, 2007

25. Schramm-Baxter, J. and Mitragotri, S. Investigations of Needle-free Jet Injections, *Proc. 26th Annual Conference of the IEEE EMBS*, 2:3543-3546, 2004.

9.0 Appendix

Selected part drawings of LLA components

REVISION HISTORY			
REV	DESCRIPTION	DATE	APPROVED

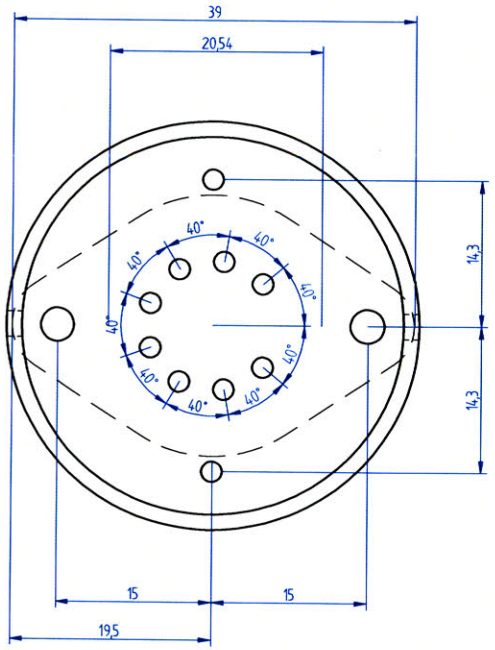

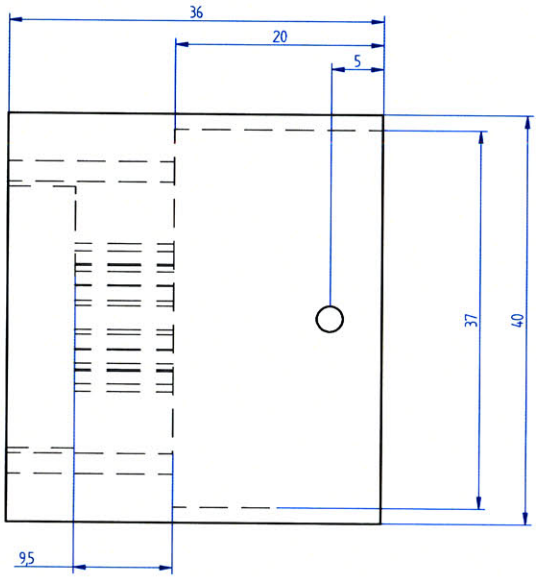

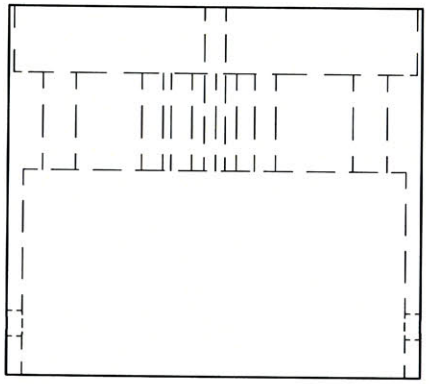

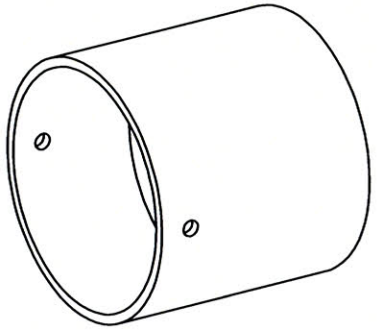

	NAME	DATE
DRAWN	Nate Ball	07/01/07
CHECKED		
ENG APPR		
MGR APPR		

UNLESS OTHERWISE SPECIFIED
DIMENSIONS ARE IN MILLIMETERS
ANGLES ±X.X°
2 PL ±X.XX 3 PL ±X.XXX

SOLID EDGE
UGS - The PLM Company

TITLE

SIZE	DWG NO	REV
A2		

FILE NAME: aluminum amp mount.dft

SCALE:	WEIGHT:	SHEET 1 OF 1

REVISION HISTORY			
REV	DESCRIPTION	DATE	APPROVED

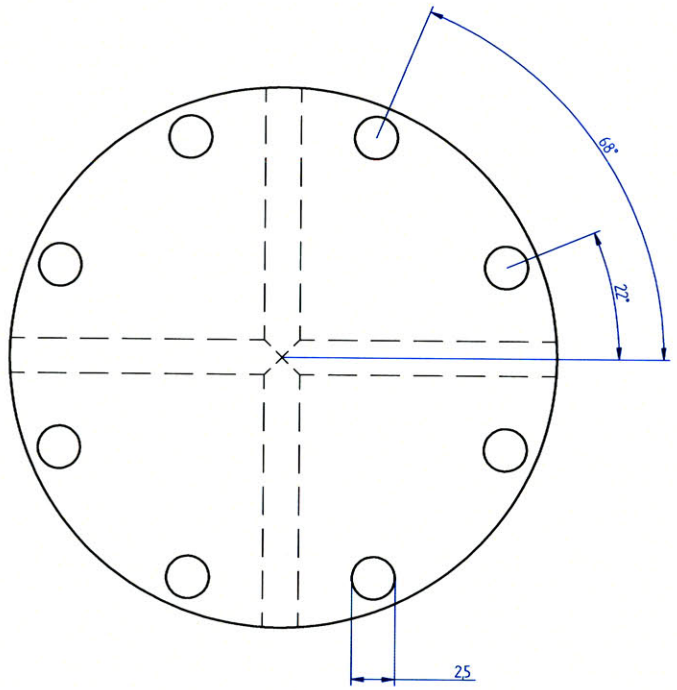

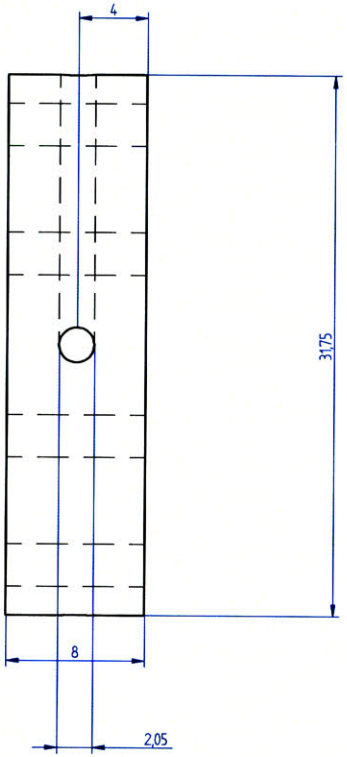

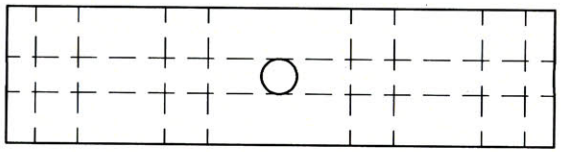

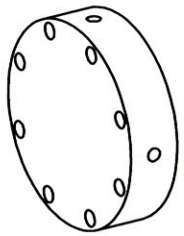

	NAME	DATE
DRAWN	Nate Ball	07/01/07
CHECKED		
ENG APPR		
MGR APPR		

UNLESS OTHERWISE SPECIFIED
DIMENSIONS ARE IN MILLIMETERS
ANGLES ±X.X°
2 PL ±X.XX 3 PL ±X.XXX

SOLID EDGE
UGS - The PLM Company

TITLE

SIZE A2 | DWG NO | REV

FILE NAME: end plate.dft

SCALE: | WEIGHT: | SHEET 1 OF 1

REVISION HISTORY			
REV	DESCRIPTION	DATE	APPROVED

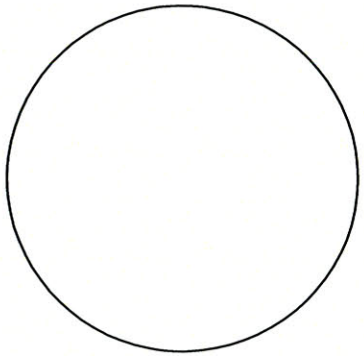

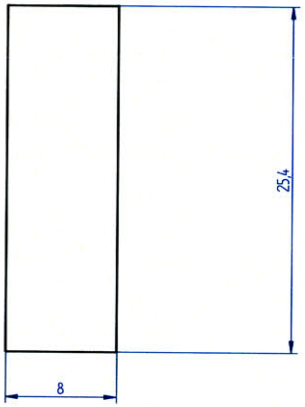

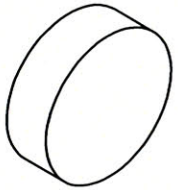

	NAME	DATE
DRAWN	Nate Ball	07/01/07
CHECKED		
ENG APPR		
MGR APPR		

UNLESS OTHERWISE SPECIFIED
DIMENSIONS ARE IN MILLIMETERS
ANGLES ±X.X°
2 PL ±X.XX 3 PL ±X.XXX

SOLID EDGE
UGS - The PLM Company

TITLE:

SIZE	DWG NO	REV
A2		

FILE NAME: field guide.dft

SCALE:	WEIGHT:	SHEET 1 OF 1

REVISION HISTORY			
REV	DESCRIPTION	DATE	APPROVED

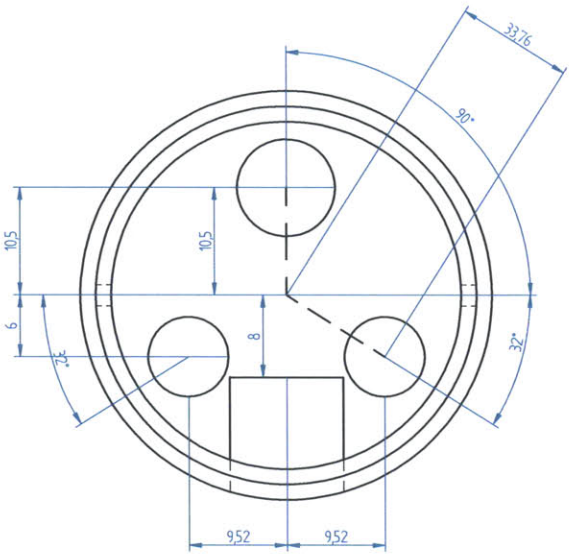

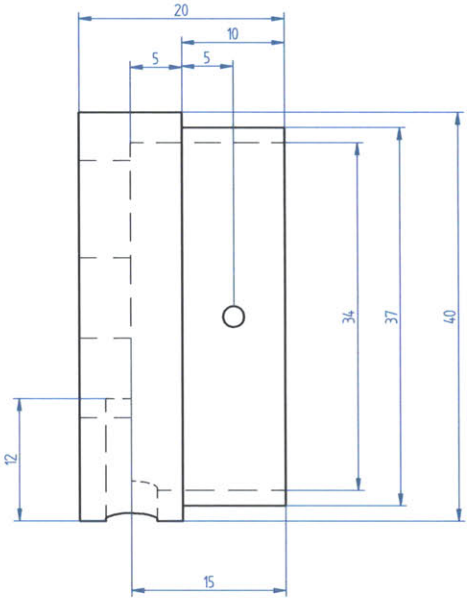

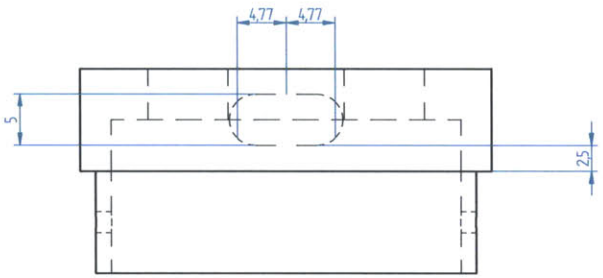

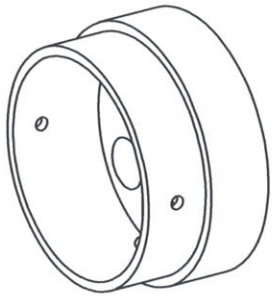

	NAME	DATE
DRAWN	Nate Ball	07/01/07
CHECKED		
ENG APPR		
MGR APPR		

UNLESS OTHERWISE SPECIFIED
DIMENSIONS ARE IN MILLIMETERS
ANGLES ±X.X°
2 PL ±X.XX 3 PL ±X.XXX

SOLID EDGE
UGS - The PLM Company

TITLE

SIZE A2 | DWG NO | REV

FILE NAME: plastic cap.dft

SCALE: | WEIGHT: | SHEET 1 OF 1

REVISION HISTORY			
REV	DESCRIPTION	DATE	APPROVED

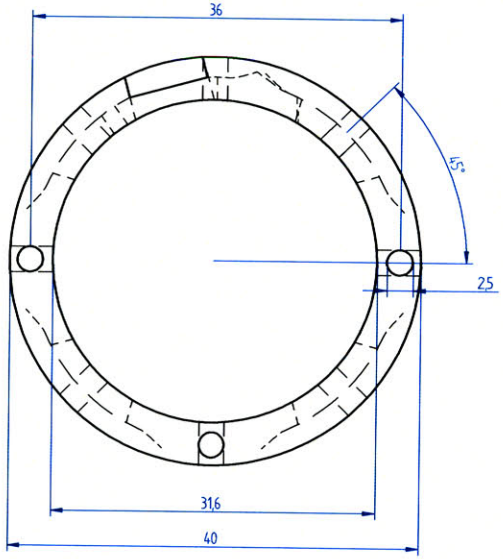

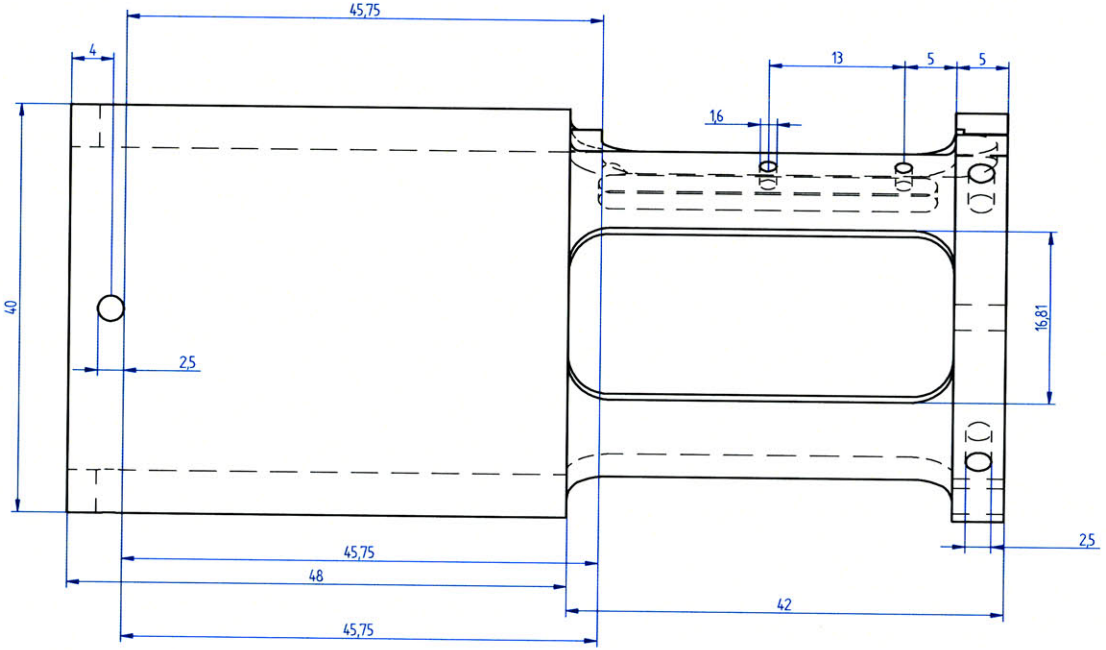

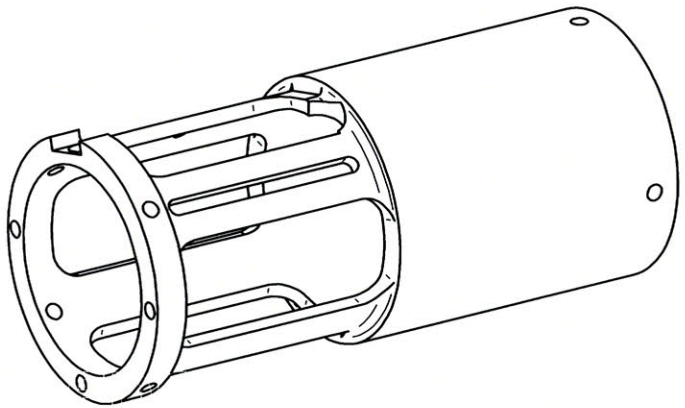

	NAME	DATE
DRAWN	Nate Ball	07/01/07
CHECKED		
ENG APPR		
MGR APPR		

UNLESS OTHERWISE SPECIFIED
DIMENSIONS ARE IN MILLIMETERS
ANGLES ±X.X°
2 PL ±X.XX 3 PL ±X.XXX

SOLID EDGE
UGS - The PLM Company

TITLE

SIZE A2 | DWG NO | REV

FILE NAME: shell.dft

SCALE: | WEIGHT: | SHEET 1 OF 1